ANTIQUITY
a review of world archaeology

CAMBRIDGE
UNIVERSITY PRESS

The Metal behind the Myths: Iron Metallurgy in the Southeastern Black Sea Region

Journal:	*Antiquity*
Manuscript ID	AQY-RE-19-076.R1
Manuscript Type:	Research
Date Submitted by the Author:	n/a
Complete List of Authors:	Erb-Satullo, Nathaniel; University of Oxford, Research Laboratory for Archaeology and the History of Art, School of Archaeology Gilmour, Brian; University of Oxford, Research Laboratory for Archaeology and the History of Art, School of Archaeology Khakhutaishvili, Nana; Shota Rustaveli State University, Department of History, Archaeology, and Ethnology
Keywords:	Chalybes, Colchis, slag, SEM-EDS, survey, smelting, technology
Research Region:	Western Asia

THE METAL BEHIND THE MYTHS: IRON METALLURGY IN SOUTHEASTERN BLACK SEA REGION

Nathaniel L. Erb-Satullo[1*]
Brian J. J. Gilmour[1]
Nana Khakhutaishvili[2]

[1] School of Archaeology, Oxford University, 1 South Parks Rd, Oxford, OX1 3TG, United Kingdom.
[2] Department of History, Archaeology, and Ethnology, Shota Rustaveli State University, 10 Rustaveli Ave, Batumi 6010, Republic of Georgia
*Corresponding Author, nathaniel.erb-satullo@arch.ox.ac.uk

Abstract

The southeastern Black Sea area is a key region for the history of iron metallurgy. Classical texts often mention the people living in this area as producers, and occasionally, inventors of iron metallurgy. Archaeological survey and scientific analysis of production debris provides the first detailed investigation of iron technologies in the region during the mid-late first millennium BC and the Medieval period. Though the dates of the sites no longer support previous claims for the earliest iron smelting, the remains do provide insight into metallurgical tradition that inspired such admiration in the Greco-Roman world.

Keywords: Chalybes; Colchis; slag; SEM-EDS; survey; smelting; technology

Introduction

The eastern and southern coasts of the Black Sea have, in a more than one sense, mythical status in the history of iron metallurgy. In the more literal sense, the region figures prominently in Greco-Roman mythical metallurgical imagination. Because of the myth of Jason and the Golden Fleece, gold is perhaps the more widely celebrated resource, but references to iron also appear, from Apollonius of Rhodes' *Argonautica* (II.1002-1008), to Aeschylus' *Prometheus Bound* (l. 714), to Pseudo-Aristotle's *On Marvelous Things Heard* (§48). In some cases, the context suggests that they are partly based on Black Sea ethnographic situation of the Classical and Hellenistic periods, contemporary with authors of these works (Hunter 1993:95). More plainly ethnohistoric accounts in Xenophon's *Anabasis* (V.5.1) and Strabo's *Geography* (XII.3.19) also mention the region's iron metallurgy. A people called the Chalybes are often mentioned as workers and perhaps even inventors of iron (e.g. Callimachus' *Aetia* IV. fr. 110.47-50, see Bittarello 2016:511-513). Though there is some debate about the historical geography of the region, and Classical accounts of the Chalybes cannot be read as purely factual, many sources locate them south or southeast of the Black Sea (Tsetskhladze 1995:321, Bittarello 2016:499-503).

The texts offer tantalizing details about the technology and organization of iron production. The *Argonautica* describes a highly specialized iron producing society that had completely abandoned agricultural pursuits in favour of metallurgical activity. A passage in *On Marvelous Things Heard* describes a production sequence involving sand and water that might be a reference to water-assisted processing of black sands to concentrate iron-rich minerals (see Khakhutaishvili 2009:107-110, 121).

In a more figurative "mythical" sense, on the other hand, archaeological evidence for iron production in the southeastern Black Sea area has proven elusive. The ancient references stimulated major speculation in the archaeometallurgical literature (Tylecote 1981, Forbes 1950:34, 453-454, Pleiner 2000:36-37, Pigott 1989:69, Yalçin 1999:184, Buchwald 2005:76, 78-79), burnishing the quasi-legendary reputation of Black Sea iron production, but leaving it largely unconfirmed. Limited archaeometallurgical field investigations in northern Turkey focused mostly on copper smelting, and the few iron smelting sites mentioned were thought to

date to the 19th century (Lutz *et al.* 1994, Seeliger *et al.* 1985:601). In western Georgia, more substantial investigations were undertaken, beginning in the early 1960s (Gzelishvili 1964). Numerous metal production sites, complete with slag heaps, furnaces, and working platforms, were excavated (Khakhutaishvili 2009). However, extensive recent fieldwork and laboratory analysis showed that they were copper smelting sites (Erb-Satullo *et al.* 2014, 2015, 2018).

Nevertheless, ancient iron smelting sites not described in Soviet-period publications were discovered during our archaeometallurgical surveys. The sites, in an area known in Classical times at Colchis, are somewhat to the east of where many scholars locate the Chalybes (**figure 1)**, but they are likely indicative of a broader southeast Black Sea metallurgical tradition. Radiocarbon dating has shown that these sites date to primarily two periods, the mid-late first millennium BC, a period roughly contemporary with the references in ancient texts, and the high Medieval period, when the Kingdom of Georgia reached its apogee as the preeminent power in the Caucasus (Erb-Satullo *et al.* 2018). This paper explores the technology and landscape-scale spatial organization of iron production during these two periods through field survey and laboratory analysis. While the main products of most of these smelting operations were likely solid state bloomery iron, some slags display features that are reminiscent of blast furnace technologies—namely, a glassy, vitreous character and phases indicative of highly reducing furnace conditions.

Survey and Chronology of Iron Smelting Sites in the Black Sea Region

Given the richness of the archaeometallurgical landscapes of the southeastern Black Sea region, and the lack of securely dated, analytically verified iron smelting remains, wide-ranging field survey was favoured over intensive excavation of any single site. Detailed information about site locations and descriptions can be found in the online supplementary materials.

One area of iron smelting was identified in the modern-day region of Samegrelo **(figure 2**). Eight iron metallurgical sites were mapped here, though Sites 78 and 83 are likely part of the same larger complex. Three of those sites were dated using charcoal fully encased within chunks of surface-collected slag. Two (Sites 80 and 83) dated to the late fifth-third centuries BC, while the other (Site 84) belongs to the Medieval period (AD 11th-12th centuries) (see full discussion of radiocarbon dates in Erb-Satullo *et al.* 2018).

Interestingly, the placement of Classical/Hellenistic period iron smelting sites within the landscape differs from the bronze industry of the Late Bronze-Early Iron Age (LBA-EIA). Site 83 (and its neighbouring Site 78) are characterized by scatters of slag at the margin of a sizable hilltop settlement, with numerous linear stone features and depressions. Iron production remains at Sites 79, 81, and 82 are similarly positioned adjacent to larger complexes with walls, mounds, ditches, and other traces of pre-modern activities. This spatial arrangement may indicate similar dates to that of Site 83, but given the absence of well-dated surface ceramics and radiocarbon dates, this is speculative. On the other hand, earlier copper smelting sites have little evidence of adjacent settlement. LBA-EIA metallurgical activities at settlement sites were restricted to secondary casting and shaping of raw metal (Erb-Satullo *et al.* 2017:121-123).

These observations may indicate that the spatial organization of metal production changed over the first millennium BC, coinciding with a series of broader social and technological changes. Increasing contact with the Mediterranean world via Greek colonies, the appearance of new materials (e.g. iron and glass), and the rise of elites, reaching their apogee in the gold-filled graves of Vani, are key developments in this period (see Kacharava & Kvirkvelia 2008). While it is not yet clear how these apparent differences in the organization of metal production fit into these broader transformations, some connection is possible.

Medieval iron smelting sites in Adjara were found at elevations of 650 to 1200 m (**figure 2**). Sixteen sites with iron metallurgical remains and one possible mining site were identified in the survey, often on very steep terrain. While some sites were heavily disturbed by modern activities, others furnished large assemblages of production debris (slags, tuyères, furnace fragments, and ores). At Site 59, for instance, a modern road cut on a steep slope exposed a 2.5 m vertical section of slag heap with three distinct phases of smelting (**figure 3**).

Mining likely took place very close to these sites. At Site 66, a large slag heap was situated immediately adjacent to clear mining remains, as evidenced by hollowed out areas of rock exposing iron-rich minerals. Other possible traces of mining were also identified farther up the ravine (Site 62). Iron-saturated water in the adjacent streams sometimes stains the downstream rocks a distinctive reddish-orange, a feature that likely aided ancient prospection.

Three sites in mountainous Adjara were dated to the Medieval period (AD 12th-14th centuries) using charcoal derived from the slag heaps (Erb-Satullo *et al.* 2018). Bayesian modelling of stratified radiocarbon dates from Site 59 indicated that the interval between the

final two smelting phases was 0-32 years (95% confidence; see online supplementary information), probably indicating seasonal use of the site over several years. Though the number of dated sites is small, these results hint that the political consolidation of Georgia in the 12th-13th centuries had economic impacts even in relatively remote mountain areas. Many Medieval-period constructions, including bridges, fortresses, and monasteries, are attested in mountainous Adjara, and the main constructions in the nearby Skhalta Church complex (**figure 2**) date to the 13th century (Chichileishvili c. 2000). Georgia suffered a series of invasions and disease outbreaks in the 13th and 14th centuries that effectively ended its regional hegemony. The latest dated iron smelting site in highland Adjara (Site 66) belongs to the 14th century, suggesting a possible connection (Erb-Satullo *et al.* 2018:176).

Iron Production Debris

Classical/Hellenistic Remains

The character of iron smelting debris at Classical/Hellenistic period smelting sites showed significant variability (**figure 4**). One type takes the form of large chunks or masses of slag. Most of these slags probably formed as slag dripped down through the hotter zones around the tuyères and solidified at the base and margins of the furnace. Other slags had flow morphologies characteristic of tap slags drained molten from the furnace. At Site 83, some tap slags were extremely glassy, ranging in colour from black to greyish blue (**figure 4 bottom centre and right**). Macroscopically, some of these slags look much more like blast furnace slags than typical bloomery slags. The quantities of glassy slag suggest that they were not a rare, accidental occurrence. None of the fully vitreous slags encased charcoal that would have permitted direct dating. However, glassy slags were found with crystalline slags, so there is little to suggest they date to a different period, at least based on surface observations. Moreover, the slag from which two radiocarbon samples came (sample 8302) was similarly low in iron, and, though not completely vitreous, contained only thin fayalite laths in a mostly glassy phase. Aside from slags, tuyère fragments with a 2-3 cm bore diameter and a 4-5 cm overall diameter, and a small fragment of ore were identified at Site 83 (**figure 5**).

Medieval Remains

Medieval iron smelting slags fell into two distinct categories. Furnace slags, which likely cooled within the furnaces, often have a curving concavo-convex shape that reflects the shape of furnace bottom. By contrast, tap slags show clear ropey flow textures and often take the form of masses of fused rivulets that cooled as they flowed from the furnace (**figure 6**).

Numerous fragments of tuyères and furnace wall were recovered. Several tuyères were fused with pieces of furnace wall, providing some indication of how the tuyères were inserted into the furnace walls (**figure 5**). Occasional finds of squared-off furnace pieces suggest that it was constructed of roughly-formed, probably un-fired, mudbricks, but no in-situ furnace structures were identified in survey.

Unsurprisingly, given the proximity of mining at Site 66, pieces of ore were identified in the slag heaps, suggesting that ore processing was also carried out here. Though the ore fragments discarded in the slag heap may have been deemed unsuitable, they nonetheless provide some information about those that were smelted.

Methods of Chemical and Mineralogical Analysis

Thirty-nine samples of slag and eight samples of ore from six sites were mounted in polished blocks for microscopic analysis. All but five samples were taken from radiocarbon-dated sites to relate technological practices securely to specific periods. Microscopic techniques were used to identify crystalline phases and describe their morphology. The presence of varying iron oxides and metallic iron in the slags can help to characterize the reducing conditions in the furnace, with magnetite ($Fe^{2+}Fe_2^{3+}O_4$), wüstite ($Fe^{2+}O$), and metallic iron (Fe^0) in slags indicating progressively more reducing environments.

Microanalysis to aid in phase identification was carried out with an energy-dispersive X-ray detector attached to the SEM (SEM-EDS). To characterize the bulk chemistry of the molten portion of the slags, area analyses were taken from a minimum of four different areas within the slag, avoiding unmelted inclusions and large voids wherever possible, and averaged together. Spot analyses of several vitreous slags were also obtained via wavelength-dispersive (WDS) electron microprobe. The identification of the chemical and mineralogical constituents of the

slags and ores help characterize the production technologies and identify the kinds of iron produced by these smelting furnaces.

Results of Slag/Ore Analysis

Classical/Hellenistic Remains

Slags from the Khobi-Ochkhomuri area contained a range of different phases and microstructures (**figure 7, table S2 in online supplementary materials**). Some slags had microstructures characteristic of bloomery smelting slag, with fayalite laths and spongy metallic iron phases. Iron oxides, predominantly wüstite and hercynite were also present. In others, however, iron oxides are virtually absent, suggesting strongly reducing atmospheres that converted virtually all "free" iron oxides not bound in the fayalite or hercynite into metallic iron (see Muralha *et al.* 2011). Lack of iron oxides and correspondingly higher silica content may also derive from melted technical ceramics or the use of lower-grade ores (Rehren *et al.* 2007). These two possibilities are not necessarily mutually exclusive, as higher temperatures, more reducing conditions, and increased melting of technical ceramics are often correlated.

A number of slags from Site 83 were either completely glassy or contained poorly-formed crystalline phases. Most of the fully vitreous slags are probably tap slags, though smaller fragments were difficult to identify with certainty. Rounded prills of metallic iron were observed in a majority of Site 83 samples. Sample 8304 contained a large cluster of rounded metallic iron prills interspersed within a matrix that is elevated in silica and aluminium relative to the main glassy phase (**figure 7D**), indicating the in-situ reduction of an ore fragment which did not fully homogenize with the rest of the melt. The uniform spherical character of the iron prills strongly suggests that at least some of them were once liquid. Etching of the prills revealed a mixture of ferrite, pearlite, and steadite suggesting the presence of phosphorus, as well as carbon up to eutectoid steel compositions (~0.8 wt% C) (**figure S5 in OSM**). Vitreous slags, especially as a major component of the slag assemblage, are atypical in bloomery smelting operations. The somewhat unusual character of the slags is also reflected in their compositions (**tables S3, S5 in OSM**), which are low in iron. This is particularly true for Site 83, where only one slag sample exceeded 40 wt.% FeO as measured by EDS. However, blast furnace slags are typically richer in

calcium, and the overall iron content, while on the low end of the typical range for bloomery slags, is significantly higher than blast furnace slags, which mostly have less than 10 wt.% FeO (Rostoker & Bronson 1990:105, Tylecote 1987:331-332). Thus, while the chemistry and microstructure of these slags share some similarities with blast furnace slags, and liquid iron was occasionally produced, it was probably not the main product of the smelt.

One reddish ore fragment was recovered from Site 83—a porous mass of hematite and other iron oxides interspersed with quartz with occasional inclusions of ilmenite, the latter of which would seem to rule out a bog iron origin (**figure 10D**). The ore sample may be consistent with a laterite deposit (see Pigott 1989:69), but investigation of the ore formations themselves would be necessary to say for sure. We found no evidence to support textual references to the exploitation of iron-rich sands (Pseudo-Aristotle, *On Marvelous Things Heard,* §48, Pleiner 2000:89).

Medieval Iron Remains

Medieval iron smelting remains also displayed significant microstructural and chemical variability (**figure 8, table S2 in online supplementary materials**). Wüstite- and fayalite-rich slags were identified, but many samples, especially furnace slags, had few iron oxide or fayalite phases. Instead, these consisted of metallic iron in a vitreous slag, sometimes with small clusters of leucite crystals, indicating strongly reducing conditions that converted all free iron oxides to metal. Often these metallic aggregates preserve relict morphologies of the ore minerals.

Small (<50 μm) iron sulphide particles were observed in many Medieval furnace slags. In one instance, iron sulphides were clearly intermingled with a cluster of iron oxides, which are either partially reacted ore or (more likely) corroded aggregates of what was once metallic iron. In either case, the micro-contextual association of these phases suggest that the sulphides were introduced to the furnace charge as a component of the ore **(figure S3 in online supplementary materials)**.

Chemically, the Medieval slags from mountainous Adjara have some notable differences from earlier slags from Samegrelo (**table S3 in online supplementary materials**). The former is characterized by a higher average calcium, sulphur, and phosphorus content, but a lower manganese content relative to the latter. These differences are likely related to the raw materials

used in smelting (predominantly ores, but perhaps also technical ceramics and fuel ash), since the Medieval slags from Samegrelo are chemically closer to the first millennium BC slags from the same region than to the slags from highland Adjara.

Etching of large iron aggregates in samples 5906 and 6606 revealed complex microstructures. Sample 6606 was characterized by large phosphorus-bearing iron grains with intergranular steadite (a Fe_3P-ferrite eutectic) and iron sulphides (**figure 9A, B**). A ~1 cm metal lump in sample 5906 has a heterogeneous microstructure indicating variable carbon, sulphur, and phosphorus content. In places, rounded pearlite colonies form a thick dendritic structure interspersed by carbon- and phosphorus-containing eutectic (equivalent to steadite or ledeburite in the binary Fe-P and Fe-C systems) (**figure 9C**). The dendritic structure suggests parts of this metal aggregate cooled from liquid state. Elsewhere in the sample appear laths of cementite with an interstitial phosphorus-containing eutectic, indicating a localized high carbon area that was also liquid (**figure 9D**). Microstructural analysis of sample 5906 demonstrates that although bloomery iron was probably the primary intended product, the furnaces were run in such a way that they did occasionally produce liquid iron. Production of liquid iron was likely facilitated by the high carbon and phosphorus content, which would have lowered the melting temperature relative to pure iron.

Analysis of seven ore samples from Site 59 and 66 revealed that they consisted of varying proportions of iron oxides and quartz (**figure 10**). Hematite is a common form of iron oxide, but various weathering products were present as well. Lath-like pseudomorphs of now-altered crystals and titanium-bearing iron oxide inclusions (likely a solid solution between magnetite and ülvospinel) were noted in sample 6601 (**figure 10A**), strongly suggesting that this sample was the formed through a process of alteration, chemical weathering, and leaching. Although low levels of sulphur were detected in all samples (especially sample 6610) via EDS, iron sulphide was never observed microscopically as a discrete phase. Comparing the Adjara ores to the ore from Samegrelo, one can see a similar pattern to that of the slags, with those of the former area having more sulphur and phosphorus but less manganese.

Discussion

Analyses of slag and other production debris show unequivocally that iron smelting took place in this region during roughly the fifth-third centuries BC and the 11th-14th centuries AD. For both periods, the quantities of slag, the presence of tap slags, the identification of relict ore microstructures, and fragments of ore all point to smelting as the primary activity, though smithing may have also taken place at some sites. Importantly, these findings conclusively rule out the possibility that metalworkers in the region merely forged raw iron imported from elsewhere. Here we have a complex iron smelting industry, operating at the same time as Classical references, with a clear mechanism of information transmission, in the form of Greek colonies and military campaigns, back to the Mediterranean world. The connection between the texts and archaeology could hardly be more clear.

The basic iron smelting technology observed in both the Classical/Hellenistic and Medieval cases is one of bloomery smelting, with some distinctive technological features. The production of liquid iron in bloomery smelting operations is well documented both experimentally and, in other regions, archaeologically (David *et al.* 1989, Tylecote *et al.* 1971:356, Charlton *et al.* 2010:365, Pleiner 2000:132). However, it is notable that some furnaces were run in such a way that they produced a) glassy low-iron slags and b) slags where most or all of the "free" iron not bound up in fayalite or hercynite was metallic iron rather than wüstite or magnetite. While some slags are more iron-rich, the proportion of vitreous low-iron slags with fewer "free" iron oxides is significant, especially at Site 83.

The recurring presence of these lower-iron, mostly glassy slags has several possible explanations, including high reducing conditions, melting of technical ceramics, and perhaps the use of low-iron, higher silica ores. Still, mostly vitreous slags often had abundant metallic iron, suggesting that the low iron content was more a product of high reducing conditions, rather than solely the melting of technical ceramics.

Higher reducing conditions does not necessarily mean that these furnaces yielded larger blooms for the same input of ore. A significant amount of metallic iron remained trapped in the slags and thus failed to coalesce into the bloom, perhaps a result of viscous, low-Fe, high-Si slags. However, low-iron slags are often associated with more carbon-enriched blooms (Tylecote *et al.* 1971, Rehder 2000:125-126, Charlton *et al.* 2010:356-357). One cost of this approach is a requirement for more charcoal per unit of ore. Given the ample forests available in the region,

this was perhaps more a question of the labour supply for charcoal production rather than of fuel availability.

While the Classical/Hellenistic sites are at present the earliest-dated iron smelting debris in the southeastern Black Sea area, iron smelting probably began somewhat earlier. Massive quantities of iron objects, in shapes suggesting local production, are found in eighth-sixth century BC mortuary complexes (e.g. Papuashvili 2012). However, the origins of iron metallurgy in the broader Near East should be sought farther southeast in Anatolia, where texts and archaeological remains point to a considerably earlier iron metallurgical tradition (see review in Erb-Satullo 2019). Unfortunately, northeastern Turkey is so poorly investigated that it is difficult to speculate about the nature of technological transmission between Colchis and Anatolia.

It is tempting to compare the mid-late first millennium BC iron smelting with late second and early first millennium BC copper smelting in the same region. The occasional appearance of iron sulphides in the slags is intriguing, as copper sulphides, iron sulphides, and iron oxides are often found in different parts of the same ore deposit. On the other hand, the association of iron smelting debris and larger complexes of walls, mounds, terraces, and ditches at Sites 78, 79, 81, 82, and 83 has no parallel at earlier copper smelting sites, and implies some organizational differences between the two industries. Specifically, iron smelting seems to have taken place adjacent to settlements, rather than in specialized sites closer to the ore deposits. These differences may reflect chronological changes in the organization of metal production over the first millennium BC, or differences between the bronze and iron industries.

Given their esteem in Greco-Roman sources, one might ask how these smelting technologies compared to those of neighbouring areas in the Near East and eastern Mediterranean. Unfortunately, contemporary iron smelting sites are lacking in these areas during both the Classical/Hellenistic and Medieval periods. Mid-late first millennium BC iron metallurgical remains have been identified in the Aegean (Photos 1989, Cevizoğlu & Yalçin 2012, Yalçin 1993), but these are mostly interpreted as smithing, not smelting remains. The lack of analyses of classical Greek iron smelting remains (Pleiner 2000:39) is particularly unfortunate. We have virtually no Aegean frame of reference, at least in terms of smelting remains, through which to view the Black Sea iron smelting traditions.

Much of the recent analytical work on iron metallurgical debris from the Near East relates to first half of the first millennium BC (e.g. Eliyahu-Behar *et al.* 2013). Tenth-ninth

century BC smelting remains at Tell Hammeh in the southern Levant are relevant, however, due to the mention of vitreous, low-iron slags at the site. These were interpreted as the result of melting of tuyères and furnace lining (Veldhuijzen & Rehren 2007, Veldhuijzen 2005:183-186, 252-253). A key difference, however, is the frequency at which these slag types appear. While at Tell Hammeh, they form about 1% of the total assemblage, they are more common at Site 83. In this respect, Site 83 is reminiscent of several late-Antique/Early Medieval smelting sites in Italy and France, where glassy low-Fe slags appear in higher frequencies at several sites (Pleiner 2000:248-249, Mahé-Le Carlier *et al.* 1998, Cucini Tizzoni & Tizzoni 2003). Site 83 may be the earliest known instance of an iron production site with these characteristics.

Medieval iron smelting has been well-studied in continental Europe (see Pleiner 2000: and references therein). On the other hand, medieval iron smelting sites in the Near East and Central Asia are poorly investigated archaeologically. As a result, it is not entirely clear where and when the blast furnace (i.e. the reduction of iron in liquid state) first appeared in the Near East and Central Asia (Craddock 2003:239-240). More analytical investigations are necessary to delineate the ways in which Medieval European, Near Eastern and Central Asian iron metallurgical traditions may have mingled in borderland regions like the Caucasus.

Conclusion

Field survey, radiocarbon dating, and analysis of production debris provide the first detailed study of iron smelting technologies in the southeastern Black Sea region, an area that in Classical and Hellenistic times achieved legendary status for its iron metallurgy. Two periods of iron smelting are documented. One, contemporary with Greek texts about the Chalybes, dates to the fifth-third centuries BC, while the other corresponds to the Medieval period (11th-14th c. AD).

The technologies of these iron smelting industries are largely based on solid-state (bloomery) smelting, though in both periods, the furnaces were run in such a way that they did occasionally produce liquid metal. Particularly at the Classical/Hellenistic Site 83, the significant quantities of glassy slag suggests that iron smelting was regularly carried out under highly reducing conditions. More research is necessary to determine how regularly liquid iron was produced, to estimate the overall phosphorus and carbon content of a typical bloom, and to

assess the degree of intentionality on the part of the metalworkers with respect to the production of liquid iron and the introduction of alloying elements. Analysis of production debris identified no evidence for the smelting of iron-rich sands, though the sites in question are not situated directly on the coast. Instead, a soft, relatively porous ore, which probably formed through a process of weathering and leaching, was used.

In evaluating the archaeological evidence against ancient sources, the discovery of mid-late first millennium BC iron smelting remains should not be taken as a literal confirmation of information about the Chalybes in Classical sources. After all, the sites investigated are slightly to the east of where many authors locate this tribe (Tsetskhladze 1995:321), and the current study found no evidence for the exploitation of iron-rich sands. At the same time, one wonders whether foreign accounts of the region's ethno-geography are an imperfect reflection of a more complicated reality. Perhaps there was some slippage between "Chalybes" as a tribe and "Chalybes" as a social group of specialized metalworkers with a broad geographical distribution in the southeastern Black Sea region. This explanation, previously suggested by others (Bittarello 2016:499n), would explain some of the ambiguities in the historical geography of the region. The idea of Chalybes as a group of specialized metalworkers also fits better with the descriptions in the *Argonautica* than their conception as a territorially-bounded discrete ethno-political unit. Given that these well-developed, complex iron-smelting industries existed precisely when contacts with the Greek world were strong and Classical texts first mention Black Sea iron smelting, it is reasonable to suggest that this archaeologically-documented metallurgical tradition provided inspiration for these accounts. These results also have implications for the investigation of Greek colonial activity in the region, as previous research argued against metals as a motivating factor, due the perceived lack of local Classical-period smelting (Tsetskhladze 1995). At present, it is not possible to say whether the iron smelting of the mid-late first millennium BC formed part of a continuous local tradition that endured through the Medieval period, or whether the metallurgical history in the region is characterized by more episodic exploitation episodes with little relationship to one another. It is only though the challenging task of finding, mapping, dating, and analysing iron smelting remains that we can delineate a more complete picture of the region that captured the metallurgical imagination of the Greco-Roman world.

Acknowledgements

The authors would like to thank Amiran Kakhidze and Anthony Gilmour for their support during fieldwork, Richard Newman (Museum of Fine Arts, Boston) who provided access to the SEM, and Victoria Smith (University of Oxford), who provided the microprobe data. Timothy Rood and Guy Westwood (University of Oxford) provided helpful comments about the texts, David Killick (University of Arizona) provided helpful advice on microscopy. Funding was provided by an NSF Graduate Research Fellowship (DGE0644491 and DGE1144152) and an NSF Doctoral Dissertation Improvement Grant (BCS-1338893), the Davis Center for Russian and Eurasian Studies, and the Jens Aubrey Westengard Fund. Digital elevation data in figure 2 are derived from ASTER (a product of METI and NASA).

Figure Captions

Figure 1. Map of the eastern Black Sea area showing survey areas (see figure 2) and modern region names.

Figure 2. Maps of metal production sites in highland Adjara and Samegrelo.

Figure 3. Drawing of section exposed by modern road cut at Site 59.

Figure 4. Slags from Classical/Hellenistic sites. Two examples of glassy slag are shown at the bottom right.

Figure 5. Examples of Medieval and Classical-Hellenistic tuyères with fused furnace material.

Figure 6. Furnace and tap slags from Medieval smelting sites.

Figure 7. Microstructures of Classical-Hellenistic slags from Sites 80 (A) and 83 (B-D) in Samegrelo. Abbreviations: Fe – metallic iron, Fy – fayalite, Ws – wüstite, Fe-S – iron sulphide, Hrc – hercynite, Gl – glassy phase.

Figure 8. Microstructures of Medieval slags from Site 59 in Adjara. Abbreviations: Abbreviations: Fe – metallic iron, Fy – fayalite, Ws – wüstite, Fe-S – iron sulphide, Hrc – hercynite, Lc – leucite, Gl – glassy phase.

Figure 9. Optical photomicrograph of iron aggregates in samples 6606 (A and B) and 5904 (C and D) from highland Adjara. Etched with Nital. Abbreviations: Fe-S – iron sulphide, Std – steadite, Prl – pearlite, Cmt – cementite.

Figure 10. SEM images of ore samples from highland Adjara (A: Sample 6601, B: Sample 6610, C: Sample 5905) and Samegrelo (D: Sample 8301). Abbreviations: Qz – quartz, Ilm – ilmenite, Fe-Ti Sp – iron-titanium spinel.

References

AESCHYLUS. 2008. Prometheus Bound, in SOMMERSTEIN, A. H. (ed.) *Persians. Seven against Thebes. Supplicants. Prometheus Bound.* (Loeb Classical Library 145): 432-563. Cambridge: Harvard University Press.

APOLLONIUS OF RHODES. *The Argonautica*, Trans. RIEU, E.V. London: Penguin.

BITTARELLO, M.B. 2016. The Chalybes as mythical blacksmiths and the introduction of iron. *Mouseion* 13: 497-534.

BUCHWALD, V.F. 2005. *Iron and steel in ancient times*. Copenhagen.

CALLIMACHUS. 1973. Aetia, in: TRYPANIS, C. A., GELZER, T., WHITMAN, C. H. (ed. and trans.) *Aetia, Iambi, Hecale and Other Fragments. Hero and Leander*. (Loeb Classical Library 421): 4-99. Cambridge: Harvard University Press.

CEVIZOĞLU, H. & YALÇIN, Ü. 2012. A blacksmith's workshop at Klazomenai, in A. ÇILINGIROĞLU & A. SAGONA (eds.) *Anatolian Iron Ages 7: Proceedings of the Seventh Anatolian Iron Ages Colloquium held at Edirne, 19-24 April 2010*: 73-97. London: British Institute at Ankara.

CHARLTON, M.F., CREW, P., REHREN, T. & SHENNAN, S.J. 2010. Explaining the evolution of ironmaking recipes – An example from northwest Wales. *Journal of Anthropological Archaeology* 29: 352-367.

CHICHILEISHVILI, M. c. 2000. *Skhalta*. Batumi: Batumi N. Berdzenishvili Research Institute.

CRADDOCK, P.T. 2003. Cast iron, fined iron, crucible steel: liquid iron in the ancient world, in P.T. CRADDOCK & J. LANG (eds.) *Mining and Metal Production through the Ages*: 207-215. London: British Museum Press.

CUCINI TIZZONI, C. & TIZZONI, M. 2003. The late Roman ironworking site at Ponte di Val Gabbia III, Bienno (Brescia, Italy), in L.C. NØRBACH (ed.) *Prehistoric and Medieval Direct Iron Smelting in Scandinavia and Europe*: 49-53. Aarhus, Denmark: Aarhus University Press.

DAVID, N., HEIMANN, R.B., KILLICK, D. & WAYMAN, M. 1989. Between bloomery and blast furnace: Mafa iron smelting technology in north Cameroon. *The African Archaeological Review* 7: 183-208.

ELIYAHU-BEHAR, A., YAHALOM-MACK, N., GADOT, Y. & FINKELSTEIN, I. 2013. Iron smelting and smithing in major urban centers in Israel during the Iron Age. *Journal of Archaeological Science* 40: 4319-4330.

ERB-SATULLO, N.L. 2019. The innovation and adoption of iron in the ancient Near East. *Journal of Archaeological Research* https://doi.org/10.1007/s10814-019-09129-6.

ERB-SATULLO, N.L., GILMOUR, B.J.J. & KHAKHUTAISHVILI, N. 2014. Late Bronze Age and Early Iron Age copper smelting technologies in the South Caucasus: The view from ancient Colchis c. 1500-600 BC. *Journal of Archaeological Science* 49: 147-159.

—. 2015. Crucible technologies in the Late Bronze-Early Iron Age South Caucasus: Copper processing, tin bronze production, and the possibility of local tin ores. *Journal of Archaeological Science* 61: 260-276.

—. 2017. Copper production landscapes of the South Caucasus. *Journal of Anthropological Archaeology* 47: 109-126.

—. 2018. The ebb and flow of copper and iron smelting in the South Caucasus. *Radiocarbon* 60: 159-180.

FORBES, R.J. 1950. *Metallurgy in Antiquity: A Notebook for Archaeologists and Technologists*. Leiden: E. J. Brill.

GZELISHVILI, I.A. 1964. *Zhelezoplavil'noe Proizvodstvo v Drevney Gruzii (Iron Smelting Production in Ancient Georgia)*. Tbilisi: Metsniereba.

HUNTER, R.L. 1993. *The Argonautica of Apollonius: Literary Studies*. Cambridge: Cambridge University Press.

KACHARAVA, D.D. & KVIRKVELIA, G.T. 2008. *Wine, worship, and sacrifice: the golden graves of ancient Vani*. Princeton, NJ: Institute for the Study of the Ancient World, in association with Princeton University Press.

KHAKHUTAISHVILI, D.A. 2009. *The Manufacture of Iron in Ancient Colchis*. (BAR International Series series 1905). Oxford: Archaeopress.

LUTZ, J., PERNICKA, E. & WAGNER, G.A. 1994. Chalkolithische Kupferverhüttung in Murgul, Ostanatolien, in R.-B. WARTKE (ed.) *Handwerk und Technologie im Alten Orient*: 56-66. Mainz: Philipp von Zabern.

MAHÉ-LE CARLIER, C., DIEUDONNÉ-GLAD, N. & PLOQUIN, A. 1998. Des laitiers obtenus dans un bas-fourneau? Études chimique et minéralogique des scories du site d'Oulches (Indre). *Revue d'Archéométrie* 22: 91-101.

MURALHA, V.S.F., REHREN, T. & CLARK, R.J.H. 2011. Characterization of an iron smelting slag from Zimbabwe by Raman microscopy and electron beam analysis. *Journal of Raman Spectroscopy* 42: 2077-2084.

PAPUASHVILI, R. 2012. The Late Bronze/Early Iron Age burial grounds from Tsaishi, in A. MEHNERT, G. MEHNERT & S. REINHOLD (eds.) *Austausch und Kulturkontakt im Südkaukasus und seinen angranzenden Regionen in der Spätbronze-/Früheisenzeit*: 65-78. Langenweißbach: Beier & Beran.

PHOTOS, E. 1989. The question of meteoritic versus smelted nickel-rich iron: archaeological evidence and experimental results. *World Archaeology* 20: 403-421.

PIGOTT, V.C. 1989. The emergence of iron use at Hasanlu. *Expedition* 31: 67-79.

PLEINER, R. 2000. *Iron in Archaeology: The European Boomery Smelters*. Praha: Archeologický ústav AV ČR.

PSEUDO-ARISTOTLE. 1936. On Marvelous Things Heard, in: HETT, W.S. (trans.) *Minor Works* (Loeb Classical Library 307): 235-325. Cambridge: Harvard University Press.

REHDER, J.E. 2000. *Mastery and Uses of Fire in Antiquity*. Montreal and Kingston: McGill-Queen's University Press.

REHREN, T., CHARLTON, M., CHIRIKURE, S., HUMPHRIS, J., IGE, A. & VELDHUIZJEN, H.A. 2007. Decisions set in slag--the human factor in African iron smelting, in S. LANIECE, D. HOOK & P. CRADDOCK (eds.) *Metals and Mines--Studies in Archaeometallurgy*: 211-218. London: Archetype.

ROSTOKER, W. & BRONSON, B. 1990. *Pre-industrial iron: Its technology and ethnology*. Philadelphia: Archeomaterials.

SEELIGER, T.C., PERNICKA, E., WAGNER, G.A., BEGEMANN, F., SCHMITT-STRECKER, S., EIBNER, C., ÖZTUNALI, Ö. & BARANYI, I. 1985. Archäometallurgische Untersuchungen in Nord- und Ostanatolien. *Jahrbuch des Römisch-Germanischen Zentralmuseums Mainz* 32: 597-659.

STRABO. 1917. *Geography, Volume I: Books 1-2* (Loeb Classical Library 49). Trans. JONES, H. L. Cambridge: Harvard University Press.

TSETSKHLADZE, G.R. 1995. Did the Greeks go to Colchis for metals? *Oxford Journal of Archaeology* 14: 307-332.

TYLECOTE, R.F. 1981. Iron sands from the Black Sea. *Anatolian Studies* 31: 137-139.

—. 1987. *The early history of metallurgy in Europe*. London: Longman.

TYLECOTE, R.F., AUSTIN, J.M. & WRAITH, A.E. 1971. The mechanism of the bloomery process in the shaft furnaces. *Journal of the Iron and Steel Institute* 209: 243-363.

VELDHUIJZEN, H.A. 2005. *Early Iron Production in the Levant: Smelting and Smithing at Early 1st Millennium BC Tell Hammeh, Jordan, and Tel Beth Shemesh, Israel.* PhD Dissertation, University College London.

VELDHUIJZEN, H.A. & REHREN, T. 2007. Slags and the city: Early iron production at Tell Hammeh, Jordan and Tel Beth-Shemesh, Israel, in S. LA NIECE, D. HOOK & P. CRADDOCK (eds.) *Metals and Mines: Studies in Archaeometallurgy*: 189-201. London: Archetype Publications.

XENOPHON. 1998. *Anabasis* (Loeb Classical Library 90). Trans. BROWNSON, C. L., Rev. DILLERY, J. Cambridge: Harvard University Press.

YALÇIN, Ü. 1993. Archäometallurgie in Milet: Technologiestand der Eisenverarbeitung in archaischer Zeit. *Istanbuler Mitteilungen* 43: 361-370.

—. 1999. Early iron metallurgy in Anatolia. *Anatolian Studies* 49: 177-187.

[Online Supplementary Materials]

The Metal Behind the Myths: Iron Metallurgy in the Southeastern Black Sea Region

Nathaniel L. Erb-Satullo[1*]
Brian J. J. Gilmour[1]
Nana Khakhutaishvili[2]

[1] School of Archaeology, Oxford University, 1 South Parks Rd, Oxford, OX1 3TG, United Kingdom.
[2] Department of History, Archaeology, and Ethnology, Shota Rustaveli State University, 10 Rustaveli Ave, Batumi 6010, Republic of Georgia
*Corresponding Author, nathaniel.erb-satullo@arch.ox.ac.uk

Survey of Metallurgical Sites

Survey of metallurgical sites in western Georgia posed a number of methodological challenges. Because the methods of systematic survey were wholly unsuitable for these hilly, densely-vegetated landscapes, survey relied upon unpublished Soviet-period field notebooks and local informants. The table below (**table S1**) provides further detail on the spatial position and character of metallurgical sites identified on survey. Sites were characterized by a concentration of metallurgical debris, primarily slag but also including tuyères, furnace fragments, and sometimes discarded ore fragments. Non-technical ceramics (i.e. ceramics not directly involved with the smelting process), which might have provided diagnostic chronological information, were rare. Because of heavy vegetation in these landscapes, the majority of sites were identified because they had been encountered during modern road-building or agricultural activities. As a result, preservation and surface exposure sometimes varied significantly. The type of metal produced at these sites was identified by a combination of macroscopic examination, qualitative portable X-ray fluorescence (pXRF) analysis (to check for the presence or absence of diagnostic metal elements such as copper or lead), and intensive optical microscopy and SEM-EDS analysis.

Traces of ancient activities besides smelting was identified near several smelting sites (**figure S1**). Several examples of possible smithing hearth bottoms were noted (e.g. at Sites 84

and 77, see **tables S1 and S2**). Unequivocal mining activities were identified at Site 66 adjacent to the slag heap, and a possible mining area was identified farther up the same ravine at Site 62. Smelting debris at a number of sites in Samegrelo was discovered in association with larger complexes including linear stone features, terraces, and mounds. Often the smelting debris would be found on the margins of these complexes, situated on lower slopes. Thick grassy turf and other vegetation precluded surface collection of ceramics to accurately date these remains. Nevertheless, it is noteworthy that the spatial association of smelting remains with larger complexes of walls, terraces, and mounds was observed at a number of Samegrelo sites (78, 79, 81, 82, 83), the last of which was dated by slag-encased charcoal to the mid-late 1st millennium BC. Nothing similar has been recorded at earlier Late Bronze-Early Iron Age copper smelting sites, or at Medieval iron smelting sites in Adjara. Naturally, more intensive investigation at these sites would be necessary to pin down the chronological development of these complexes, but it is conceivable that they reflect a spatial organization of iron metallurgy that is specific to the mid-late 1st millennium BC.

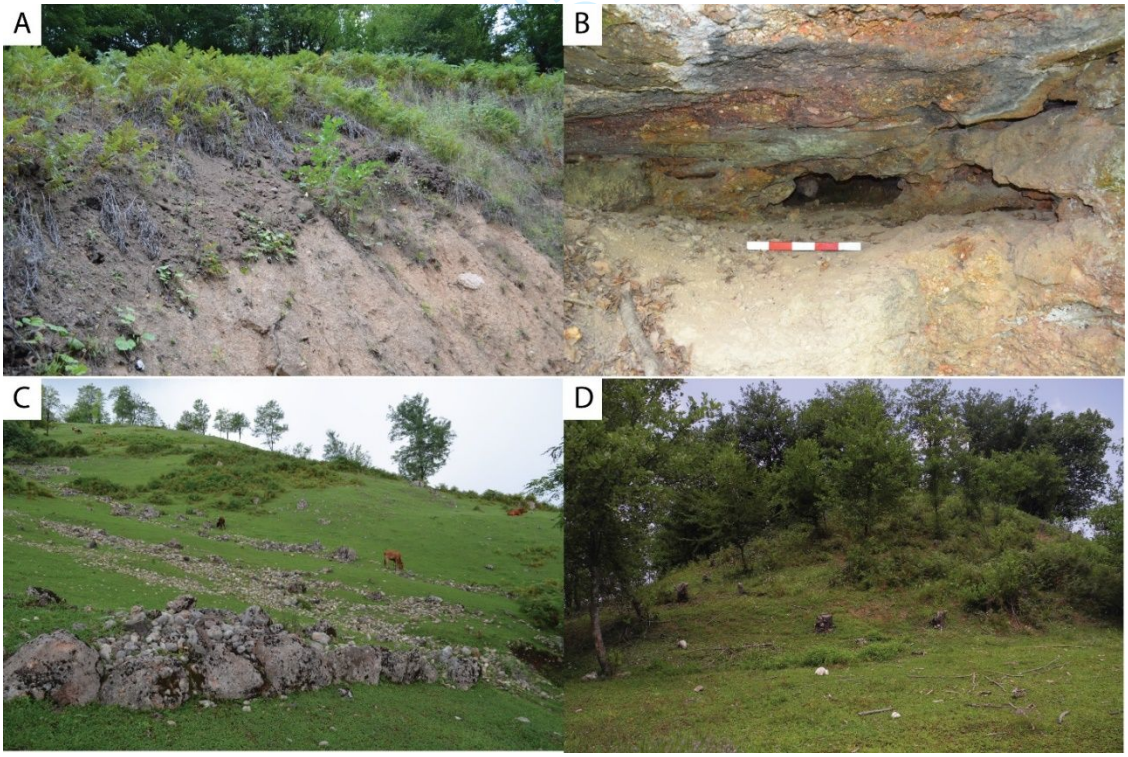

Figure S1. Slag heaps and other features identified on survey. A. Eroded portion of slag heap (dark grey deposit) at Site 66. Mining activity shown in (B) was found at the tree-line in the background. B. Traces of ancient mining activity at Site 66. Scale bar is 50 cm. C. Linear stone features on hill above smelting sites 83 and 78. D. Anthropogenic mound on hill above smelting debris at Site 79.

Table S1. Metallurgical sites identified in mountainous Adjara and Samegrelo areas. Coordinates are given in UTM Grid 38N.

Site #	Site Name	Easting	Northing	Site Type	Site Description
57	Tago I	275754	4610779	Fe Smelting Site	Disturbed site in garden plot behind a house. Poor visibility and exposure.
58	Tago II	275688	4610644	Fe Smelting Site	Slag scatter spread over gently sloping ground with short grass and maize field.
59	Dzmagula I	274353	4609024	Fe Smelting Site	Slag heap on very steeply sloping ground, cut by road construction. Large exposed section of slag heap visible. Rest of site likely covered by landslides.
60	Chao I	274405	4610996	Fe Smelting Site	Heap of tap and furnace slag, likely disturbed by land clearance for small agricultural fields.
61	Cheri I	276035	4607972	Fe Smelting Site	Tap and furnace slag in road cut near cemetery.
62	Gurdzauli I	276718	4609203	Fe Mining Site (?)	Possible debris heap from mining in stream bed. Iron-rich water in stream has stained downstream rocks red. A single small piece of slag was found in the adjacent roadway.
63	Dzmagula II	274337	4609248	Fe Smelting Site	Scatter of slag (highly disturbed) in garden plot. Large pieces were collected by farmers and piled on the upslope edge of the field.
64	Tsablana I	280144	4607897	Fe Smelting Site	Dense accumulation of slag at bottom of very steep west-facing hillslope. In field above, a slight bulge in the slope is visible, indicating the likely extent of the slag heap. Tap slag predominates in the artifacts visible at the surface.
65	Tsablana II	279970	4607240	Fe Smelting Site	Highly disturbed smelting site in maize field, with cairn of slag produced by recent agricultural clearance. Small fragment of obsidian found nearby.

66	Cheri II	276218	4608054	Fe Mining and Smelting Site	Large slag heap on steeply sloping ground. Nearby landslip has partially eroded the slag heap, but the remainder seems relatively undisturbed. Above the slag heap, small mining galleries were identified, which cut into the exposed rock outcrop.
67	Kinchauri I	277895	4606339	Fe Smelting Site	Large scatter of slag in agricultural field. Tap and furnace slags as well as technical ceramics and possible ore. Undisturbed slag heap not identified.
68	Dzmagula III	275001	4609298	Fe Smelting Site	Scatter of slag (mostly dense with one possible piece of tap slag) in agricultural fields. Deposits likely disturbed.
69	Pachkha I	278436	4609322	Fe Smelting Site	Disturbed slag deposits in agricultural fields and roadways on SSE facing hillside.
70	Pachkha II	278327	4609325	Fe Smelting Site	Disturbed scatter of slag found on either side of road and (according to local villagers) in neighbouring maize field.
71	Pachkha III	277702	4609087	Fe Smelting Site	Well preserved slag heap on S facing slope in woodland.
72	Tsablana III	279141	4606910	Fe Smelting Site	Smelting site partially damaged by road building. Slag scattered downhill from road cut.
73	Cheri III	275621	4608165	Fe Smelting Site	Pieces of slag found in roadway. Pieces are small enough and scarce enough that it is possible they come from higher up on the slope. Further investigation needed.
74	Chogha I	270751	4716817	Cu Smelting Site	Previously excavated site dated to the first half of the first millennium BC with both spongy and dense slag cake fragments. Site located in overgrown tea plantation, but a pile of slag 3-4 m in diameter (likely piled up in process of excavation) is clear of vegetation. See Khakhutaishvili (2009:95-104) for more details.
75	Chogha II	271016	4716981	Cu Smelting Site	Previously excavated site dated to the first half of the first millennium BC in dense vegetation of an overgrown tea plantation. Spongy and dense slags present, along with technical ceramic. See Khakhutaishvili (2009:95-104) for more details.

76	uncertain	268939	4716065	Metal Production and possible settlement	Small pieces of pottery, slag and flecks of charcoal exposed in road cut by Ochkhomuri River. Unclear whether this is an in-situ deposit or hillwash from a site farther up the slope. Site 76 and Site 77 might be part of the same settlement complex. Khakhutaishvili (2009:95) mentions an unexcavated Iron Age settlement somewhere close by; sites 76 and 77 may part of that site.
77	uncertain	269082	4716118	Iron production (smithing?) and possible settlement	Several pieces of slag (one potential smithing hearth bottom) and a tuyère found on slopes. Likely material eroded from densely vegetated area higher up on the slope. Local villagers reported finding ceramics when planting hazelnut trees in the vicinity. Site 77 and Site 76 may be part of the same general complex. Khakhutaishvili (2009:95) mentions an unexcavated Iron Age settlement somewhere close by; sites 76 and 77 may be part of that site.
78	Zumi I	266349	4720875	Fe Smelting near Settlement	Iron smelting slag scattered in a maize field. Highly disturbed but likely part of the larger settlement and smelting complex along with Zumi II. Tap slag is very glassy.
79	Nakiani I	269674	4711512	Fe Smelting and Settlement	Light scatter of metallurgical remains on hillslope below a terraced area and mound on hilltop. Mound is similar to that found at Site 81, but its purpose is unclear.
80	Jumiti I	264413	4714499	Fe Smelting Site	Significant scatter of slag on sloping ground above Khobi River.
81	Napichkhovo I	271618	4719981	Fe Smelting and Settlement	Diffuse scatter of slag over large area over cultivated and grazing land. Smelting activities are clearly part of a larger complex, with leveled terraces, a hilltop mound, and ditch cut into bedrock. Possible evidence of collapsed stone architecture, but very poor ground visibility made it difficult to assign a date. A possible fragment of mortared masonry was identified.
82	Naukhramu I	274643	4721730	Fe Smelting Site w/other structures	Thinly scattered slag in dense forested area with evidence of stone architecture. Surface visibility extremely poor, and dating of these features is unclear.

83	Zumi II	266229	4720846	Fe Smelting and settlement	Substantial quantities of slag (often with quite glassy appearance) spread over a large area. Likely part of the same complex as Site 78—they are quite close. Much slag is glassy, and tuyère fragments were identified. Above the slag scatter, there are a number of terraces, with some evidence of stone architecture. A few small fragments of coarse unidentified ceramics were found here. Evidence for settlement is spread over several adjacent rises above the smelting remains of Sites 78 and 83.
84	Jumiti II	263541	4713560	Fe Smelting with possible smithing	Large low-density scatter of slag likely disturbed by plowing for agricultural activities. Finds include some possible smithing hearth bottoms and tap slags.

Radiocarbon Dating of Sites

Dating metallurgical sites identified on survey was of paramount concern. Diagnostic non-metallurgical ceramics were rarely found on these sites. Radiocarbon dating of charcoal, either from exposed sections or encased within surface collected slags, proved an effective dating strategy. Detailed discussion of the radiocarbon dates on iron smelting remains has been reported in another publication (Erb-Satullo *et al.* 2018), but a table of iron smelting dates is included here (**table S2)**. However, additional Bayesian modelling of the dates on charcoal recovered from stratified deposits from Site 59 was undertaken for this paper, as it illustrated the rate of deposition in the slag heap and carried implication for seasonality in iron production in mountainous Adjara. Incorporation of stratigraphic information into the priors using OxCal showed that periods of abandonment were quite short. Samples were taken from contexts 1002 and 1005, which were part of two distinct phases of metallurgical activity at the site separated by a layer of slag-poor sediment 20-40 cm thick. Even prior to dating, it was hypothesized that these layers were deposited in relatively quick succession, and the layer of slag-poor sediment was identified as fill from the digging out of a furnace and flat workspace on what was otherwise steeply sloping ground. Radiocarbon dating confirmed that the interval between phases of smelting was quite short. Bayesian modelling of three dates (OxA-30108, OxA-30109, and OxA-30110) suggests that the length of time between the deposition of contexts 1005 and 1002 (which included deposition of a slag-poor buff-coloured sediment, 1003 in between the slag-rich deposits) was between 0 and 32 years (95.4% confidence). The probability density curve (**figure S2**) is positively skewed with a maximum at about 2 years, meaning that the interval is far more likely to be less than 16 years than it is to be between 16 and 32 years. These results suggest that smelting took place seasonally, and fairly large amounts of slag were deposited quickly. The picture of seasonal smelting is entirely consistent with the setting of these sites, situated on steep ground in mountain ravines with significant winter snowfall. Accurately assessing the overall scale of production is difficult, as the total volume of the slag heap was impossible to estimate, since colluvial sedimentation and vegetation obscured the parts of the slag heap that were not exposed by the modern road cut.

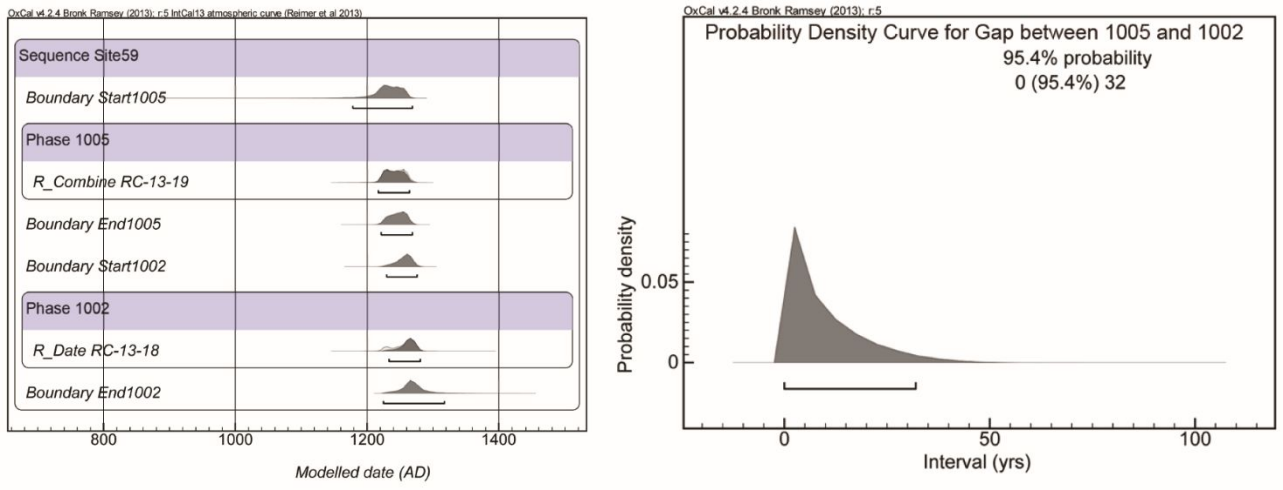

Figure S2. Bayesian modelling of interval between the deposition of 1005 and 1002. See main article for a drawing of the stratigraphic section.

Table S2. Table of radiocarbon dates from iron smelting sites. Dates from Erb-Satullo *et al*. (Erb-Satullo *et al.* 2018:174).

Field #	**Lab #**	**Site #**	**Material**	**Uncalibrated Date (RC yrs BP)**	**Calibrated 2σ Date Range**
RC-13-18	OxA-30108	59	*Fagus sylvatica; Corylus; Castanea/Quercus* wood charcoal	766±23	AD 1222-1280
RC-13-19a	OxA-30109	59	*Juglans regia* wood charcoal	777±23	AD 1220-1276
RC-13-19b	OxA-30110	59	*Juglans regia* wood charcoal	817±24	AD 1170-1264
RC-13-32	OxA-30111	64	*Carpinus* wood charcoal	860±23	AD 1054-1079 (4.6%); AD 1152-1246 (90.8%)
RC-13-25	OxA-30112	66	*Quercus* wood charcoal	666±23	AD 1278-1315 (51.6%); AD 1355-1389 (43.8%)
RC-14-31	AA105846	80	Angiosperm wood charcoal	2349±32	516-370 BC
RC-15-5	AA107059	80	Angiosperm wood charcoal	2266±40	401-346 BC (38.9%); 321-206 BC (56.5%)
RC-14-32	AA105845	83	Angiosperm wood charcoal	2251±32	396-346 BC (31.7%); 321-206 BC (63.7%)
RC-15-8	AA107058	83	Angiosperm wood charcoal (likely *Quercus*)	2300±27	406-357 BC (84.2%); 285-235 BC (11.2%)
RC-14-33	AA105844	84	Angiosperm wood charcoal	947±30	AD 1025-1155

Further Details on the Microscopic and Chemical Analysis of Slag Samples

Understanding the chemistry and mineralogy of slag samples was essential for understanding the type of metal produced, the ores used, and the thermodynamic conditions within the furnace. Microscopic associations between different phases, such as the association between iron sulphides and iron oxides/iron metal (**figure S3**), can indicate that such materials were added to the charge together. Finds of vitreous (i.e. glassy) or poorly crystallized slags, were a notable feature of both slags from both periods, but were particularly notable at Sites 78 and 83, the latter of which was radiocarbon dated to the Classical/Hellenistic period (**figure S4**) Vitreous slags are characterized by the absence (or minimal presence) of crystalline phases (e.g. iron silicates such as fayalite) in the portion of the slag that was once fully molten. Vitreous slags typically have lower iron and more elevated silica content relative to slags with substantial crystalline phases. Occasionally, areas of devitrification, with tiny crystals that are barely resolvable via optical microscopy, are visible in glassy slags, but these are easily distinguished from the formation of larger crystalline phases.

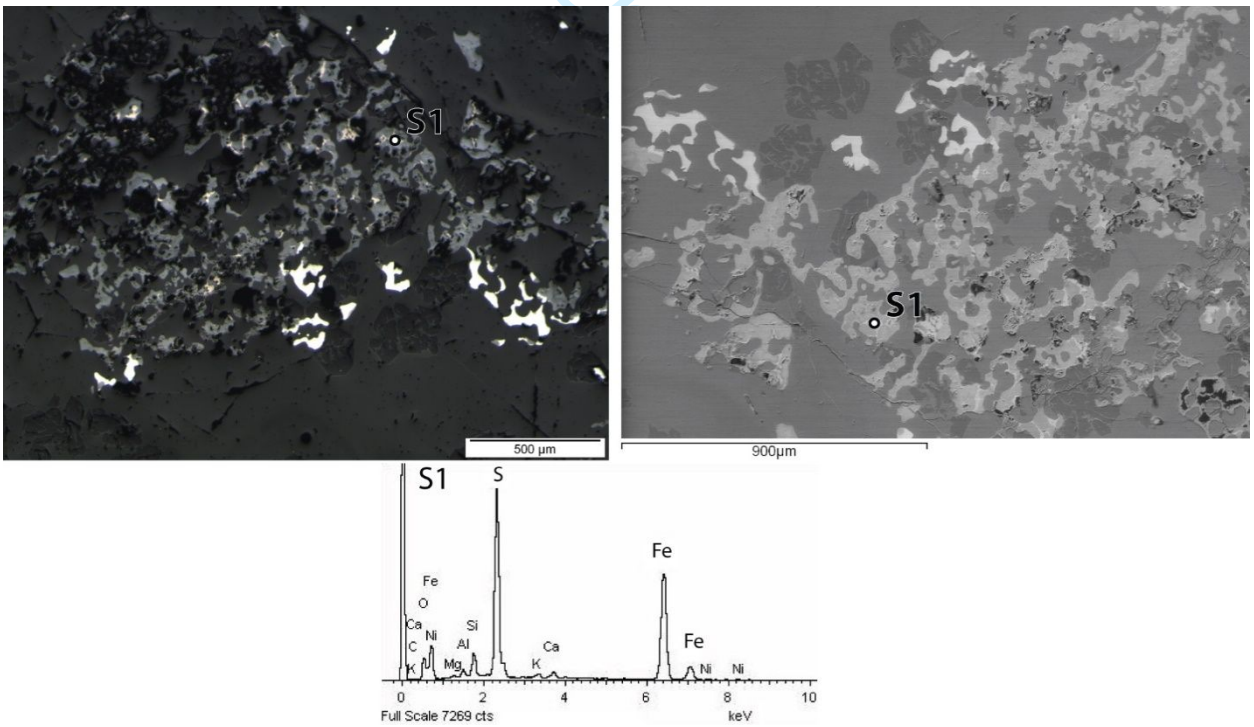

Figure S3. Optical photomicrograph (left) and scanning electron image (right) of iron sulfides finely intermixed with iron metal and iron oxides in sample 5904, along with an EDS spectrum of the iron sulfide phase.

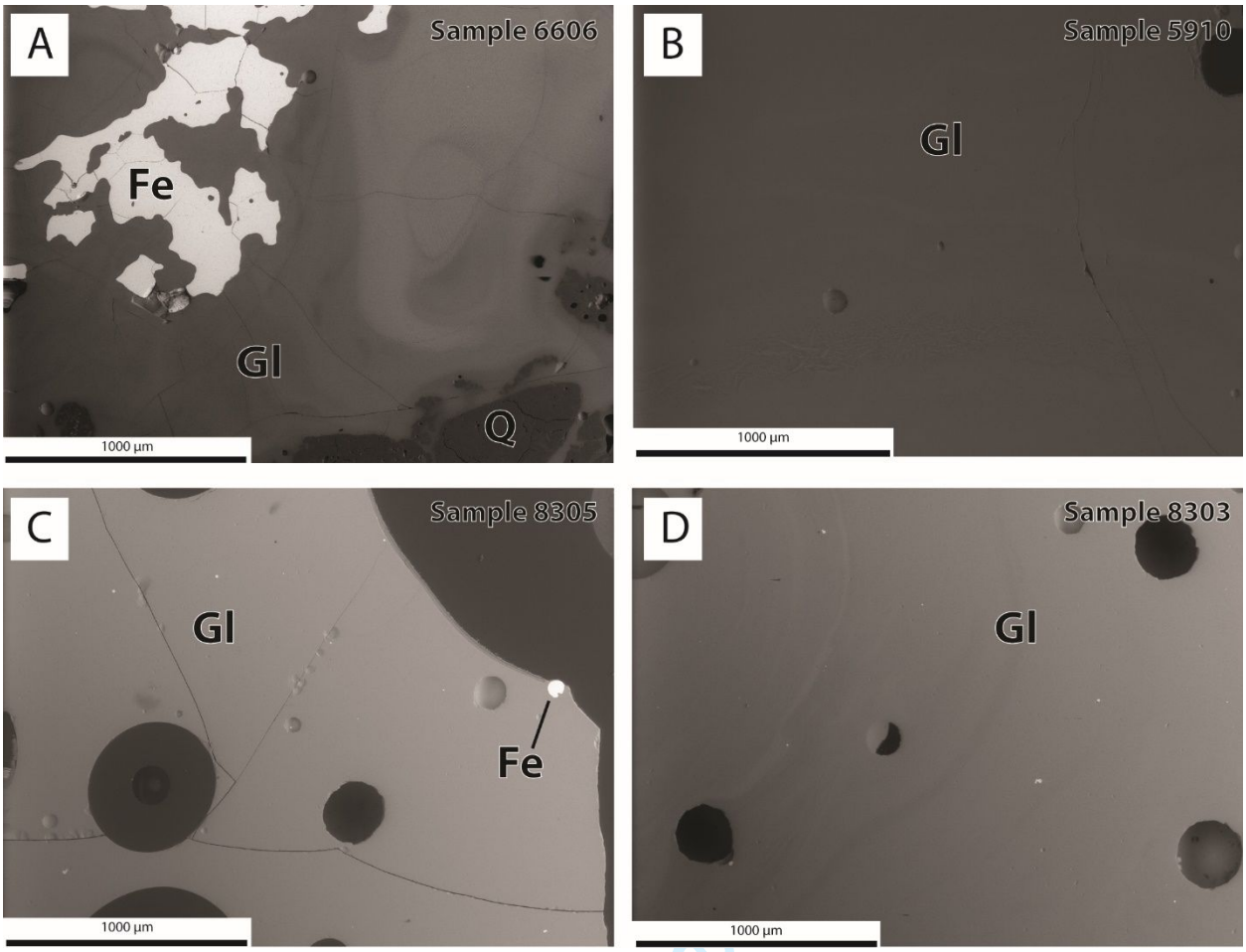

Figure S4. Examples of microstructures of vitreous slags. Dark circular areas are gas bubbles. Abbreviations: Fe – metallic iron, Q – quartz, Gl – glassy phase.

Table S3 lists macroscopic slag type, the presence or absence of certain key phases and other features, and a general microscopic description of each sample as determined by optical and scanning electron microscopy. In cases where the presence is loosely quantified, the categories are "present in significant amounts" (XX), "present in a few instances" (X), and "not identified" (—). "Free" iron oxides refer to magnetite and wüstite crystals forming from the melt, which are indicators of the redox conditions at the time of their formation. Not included in this category are iron oxides that formed from the post-depositional corrosion of what was once metallic iron, and hercynite, which is categorized separately. The former is distinguishable based on microstructure and the presence of occasional islands of uncorroded metal. The latter is identifiable due to its low optical reflectance and high aluminium content in SEM-EDS spot analyses. Strictly speaking, in most cases this phase is likely a hercynite-rich solid solution with

a composition between pure hercynite ($FeAl_2O_4$) and pure magnetite (Fe_3O_4), which forms a complete solid solution above 850°C (Muralha *et al.* 2011:2081). Relict ore morphologies are clusters of iron oxide or iron metal which preserve textures or shapes that are reflective of the original ore. These structures tend to occur in areas where reduction was either incomplete, or the melt cooled before the reduced metal coalesced into the bloom.

The morphology and microstructure of the metallic iron phases is an important indicator of the technological process. Typical bloomery smelting slags, particularly furnace slags, often contain aggregates of metallic iron—metal that did not coalesce with the larger bloom. By contrast slags associated with liquid iron technologies (blast furnace or crucible steel slags, for instance) will often trap small prills of iron. Etched microstructures of metallic iron particles within the slags can reveal compositional information and provide further indications of whether the metal cooled in solid or liquid state. In the heterogeneous environment of the pre-modern smelting furnace, the composition of small particles of metallic iron are not necessarily the same as the overall composition of the iron produced, but they can serve as general indicators of the type of metal produced (see Erb-Satullo *et al.* 2015:268).

While much of the metallic iron identified in the slags is typical of bloomery smelting slags, several samples displayed unusual microstructures. A fragment of reduced ore that failed to fully homogenize with the slag metal was identified in Sample 8304 (of Classical/Hellenistic date), and the presence of dozens of small round prills of iron (**figure S5)**. Rounded particles of iron can form even in a solid state process, by the nearly perfect spherical character of some prills (**figure S5 C**) suggests at least some of them were molten. Upon etching, however, most seemed to be predominantly phosphorus-bearing ferrite, while others had a mixture of ferrite and pearlite and one was entirely pearlite. Evidence of spheroidization was visible in the pearlite structures, indicating a slow cooling process. Another prill also contained a net-like structure of steadite, indicating high phosphorus content and cooling from a liquid state.

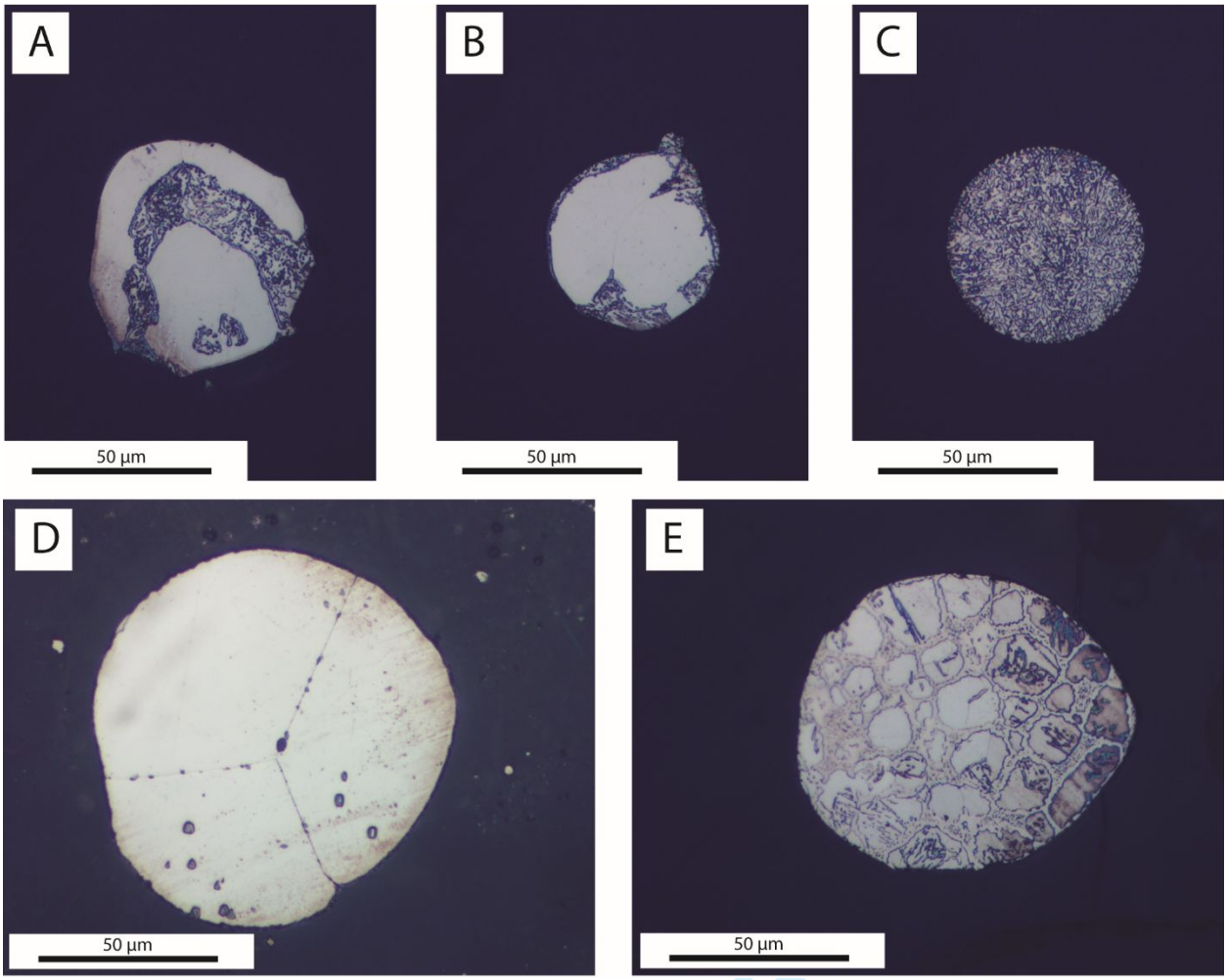

Figure S5. Optical photomicrographs (PPL) of round iron prills in 8304. A, B – ferrite and pearlite with some spheroidization; C – pearlite (spheroidized); D – large grained phosphoric ferrite; E – ferrite, (spheroidized) pearlite, and steadite eutectic.

The metallic aggregate in sample 5906 (of Medieval date) also displays a complex microstructure with significant carbon and phosphorus content, which varied considerably across the sample (**figures 9 and S6**). In some areas, rounded colonies of pearlite arranged in lines approximates a thick dendritic structure (**figure S6C)**, with a well-developed eutectic interspersed between them. In one area, the carbon content was so high enough to induce the formation of cementite laths with pearlite and a eutectic containing both carbon and phosphorus (**figure S6B**). This microstructure is a product of the ternary Fe-C-P phase diagram, and the eutectic cannot be adequately explained as either steadite (the eutectic of the Fe-P system

consisting of ferrite and iron phosphide) or ledeburite (the eutectic of the Fe-C system consisting of austenite and cementite, which converts to pearlite and cementite as the metal cools). This eutectic consists of a phosphide phase, but it is clear that at least some of the small blebs within it are pearlite rather than ferrite. The laths of cementite present in the sample indicate a high carbon content and are reminiscent of proeutectic cementite seen in cast irons with >4.3% C. The presence of pearlite colonies in this however, is not consistent with a hypereutectic (>4.3% C) cast iron, so the phosphorus must play a role in the formation of what would otherwise be a contradictory microstructure. Other areas of the sample have lower quantities of phosphorus and carbon, with no eutectic structures. As a whole, these microstructure can be interpreted as evidence of localized melting induced by high carbon and phosphorus content. Some caution is warranted, however, when discussing composition of the overall metal product of these furnaces. While, it is likely that the iron metal contained both carbon and phosphorus, it is difficult to extrapolate quantitative data from this small aggregate. The ~1 cm diameter aggregate in 5906 was the largest piece of metal identified in any of the slags, but spongy metallic aggregates, consisting largely of ferrite, were identified in other samples. Even more caution in inferring the composition of the overall product is warranted with the round prills from sample 8304, which are even smaller. More research is necessary, both on finished products and on metal in slags, to narrow down compositional estimates for the typical type of metal produced at these sites.

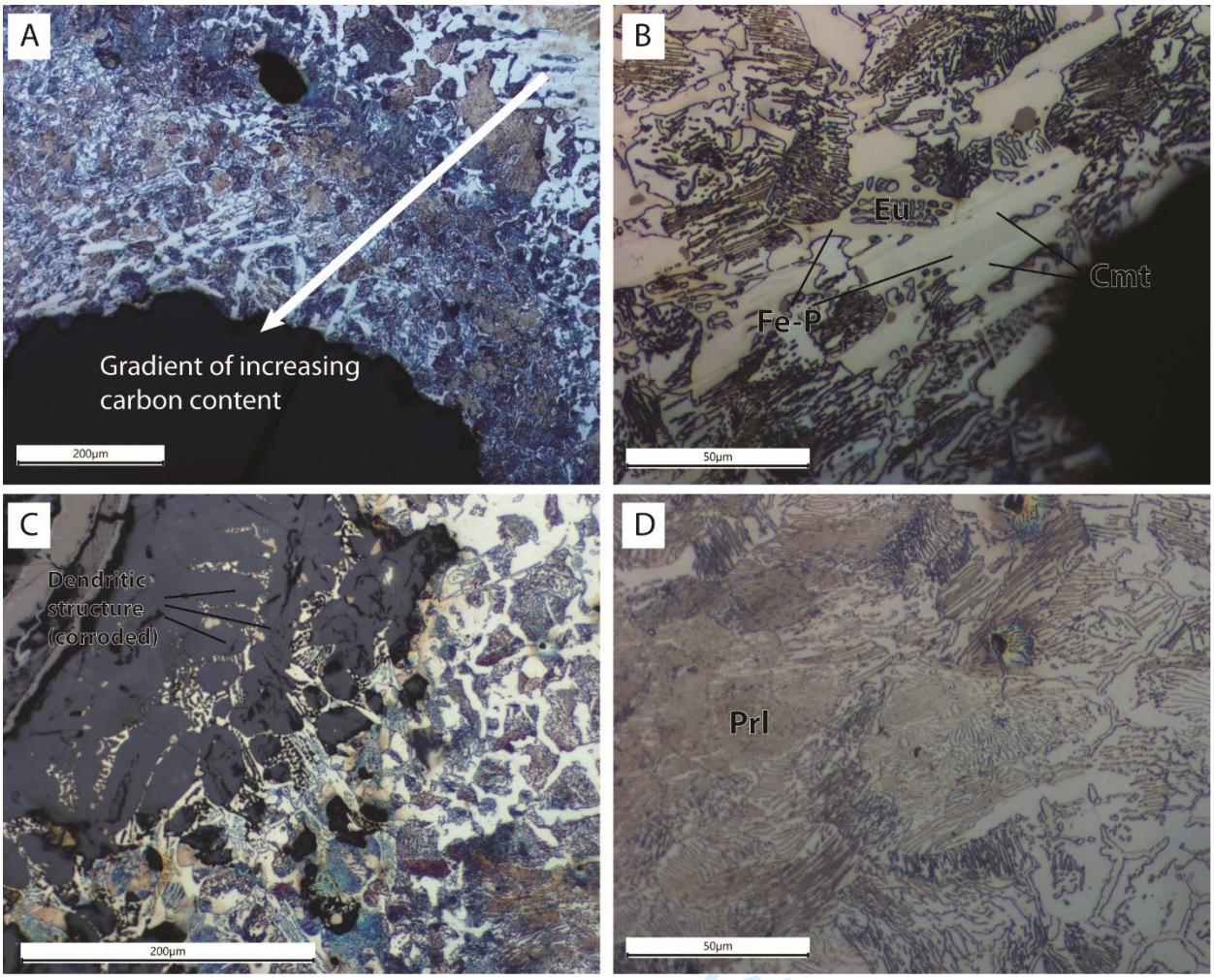

Figure S6. Additional optical photomicrographs of metal aggregate in Sample 5906 etched with Nital, showing variable carbon and phosphorus content throughout the sample. Abbreviations: Fe-P – iron phosphide, Eu – ternary Fe-C-P eutectic structure, which includes iron phosphide as a constituent phase, Cmt – Cementite.

Table S3. Mineralogy and microstructures of all slags analysed by optical microscopy. Abbreviations: FS – furnace slag (a product of smelting) SHB – Smithing hearth bottom (a product of iron smithing), TS – Tap Slag (a product of smelting), I – indeterminate type (usually for small fragments), XX – present in significant quantities, X – present, but in only a few instances, (—) – not observed. Entries of "none" or "minimal" in the iron oxide form column indicate that iron oxides are absent or virtually absent in the sample.

Sample Number	Period	Type	Dominant Form of "Free" Iron Oxides	Metallic Iron	Hercynite (Al-rich Spinel)	Relict ore morphologies	Iron Sulphides	Iron Phosphides	Description
5701	Probable Medieval	FS	Magnetite/Wüstite	XX	XX	XX	—	—	Heavily corroded, very heterogeneous slag. Iron oxides are predominantly in relict ore morphologies, but wüstite and magnetite were both observed. Lots of corroded metallic iron aggregates.
5702	Probable Medieval	TS	None	XX	XX	—	X	—	Mostly glassy slag with thin iron silicate laths and rounded prills of metallic iron.
5801	Probable Medieval	FS	Wüstite	XX	XX	X	—	—	Wüstite heavy slag with some leucite, and possible relict ore morphologies. Fairly corroded.
5802	Probable Medieval	TS	Wüstite	XX	XX	—	—	—	Wüstite and fayalite-dominated slag with some hercynite.
5901	Medieval	FS	Wüstite	XX	X	—	—	—	Large quantities of wüstite along with a number of particles of metallic iron.
5902	Medieval	TS	Wüstite/Magnetite	—	XX	—	—	—	Iron silicate laths with tapping bands of iron oxides. Overall little iron oxide, some leucite. Magnetite seen with varying reflectance, SEM-EDS spectra show significant Al presence in some grains.
5903	Medieval	FS	Minimal	XX	X	XX	XX	—	Aggregates of metallic iron mimicking ore morphologies, many small prills of iron sulphide. Almost no magnetite/wüstite, small amount of hercynite. Cr/Ti/V detected in Hercynite crystals. Plagioclase feldspars were identified. Some of the plagioclase crystals are growing into the iron aggregates, suggesting the iron was in a liquid state as the plagioclase crystals formed.
5904	Medieval	FS	Minimal	XX	—	XX	XX	—	Aggregates of metallic iron mimicking or morphologies. Almost no magnetite/wüstite, significant leucite.
5906	Medieval	FS	Minimal	XX	—	—	XX	XX	Essentially a small bloom fragment with adhering glassy slag. Metal has abundant sulphide and phosphide phases. Highly variable microstructure.

5907	Medieval	FS	Minimal	XX	XX	XX	XX	—	Fairly corroded iron, with significant metallic iron. Anorthite-rich plagioclase feldspar present. Abundant iron sulphides. Iron oxides present are likely corroded iron. Al-rich and Ti-rich spinels present.
5910	Medieval	TS	None	X	—	—	—	—	Glassy slag with one single prill of metallic iron.
5911	Medieval	TS	None	X	—	—	—	—	Glassy tap slag with a single tiny iron prill.
5912	Medieval	FS	Minimal	XX	—	XX	XX	—	Large aggregates of metallic iron, with textures indicating solid state reduction. Minimal iron oxides, some of which appear to be corroded metal. Small prills of iron sulphides. Possible Al-rich spinels (hercynite) in one area near melted technical ceramic.
5913	Medieval	TS	Magnetite	—	—	—	—	—	Glassy slag with thin iron silicate laths and rounded prills. Few iron oxides, most of which are concentrated near surface and at tapping bands. Slight more iron oxides than 5914.
5914	Medieval	TS	Minimal	X	—	—	—	—	Glassy slag with thin iron silicate laths and rounded prills. A small amount of magnetite is visible at tapping bands. One prill of metallic iron noted.
6603	Medieval	FS	None	XX	X	XX	—	—	Large aggregates of metallic iron with leucite in a glassy phase. Minimal iron oxides (those present seem to be corroded metallic iron).
6604	Medieval	FS	Wüstite	XX	XX	XX	XX	X	Heterogeneous microstructure: large aggregates of metallic iron, leucite, fine iron oxides, some sulphides, possible steadite (iron-iron phosphide eutectic). Leucite was observed, as were some Al-rich spinels (hercynite).
6605	Medieval	FS	None	XX	—	XX	XX	—	Abundant iron aggregates, fine silicate crystals, (iron silicates, a feldspar of anorthite-rich composition) and little iron oxides. Some partially reacted quartz. Abundant iron sulphides at the grain boundaries. Phosphide not observed, but it may have been missed (sample not etched).
6606	Medieval	FS	None	XX	—	XX	XX	XX	Large aggregates chunks of metallic iron with phosphides and sulphides at grain boundaries. Large metal grains characteristic

									of phosphoric iron. Slag is highly glassy, with no freshly-formed crystalline silicate phases. Some partly reacted quartz.
6607	Medieval	TS	Wüstite	—	XX	—	—	—	Wüstite and fayalite-dominated slag with no metallic iron. Tapping bands visible.
6608	Medieval	TS	Wüstite	X or XX	XX	—	—	—	Iron silicate laths with interstitial wüstite and small particles of metallic iron. Hercynite present, as well as a small amount of Leucite.
6609	Medieval	TS	None	—	—	—	XX	—	Thin laths of iron silicate, no iron oxides/metallic iron. Very tiny prills of sulphide in between the fayalite laths.
7901	Probable Classical/ Hellenistic	FS	Wüstite	X	XX	—	—	—	Wüstite, fayalite, and hercynite. Wüstite declines closer to adhering technical ceramic. Small particles of metallic iron.
8004	Classical/ Hellenistic	FS	None	X	XX	—	XX	—	Sample microstructure varies, in large parts dominated by iron silicates and hercynite. Also present are some equiaxed angular Fe-Ti-Al spinels. A single tiny particle of metallic iron. Fine iron sulphide prills present throughout.
8005	Classical/ Hellenistic	FS	Minimal	XX	XX	—	XX	—	Fayalite-dominated slag with significant amounts of hercynite but minimal presence of other "free" iron oxides, which are only observable as minute crystals in between the large fayalite laths. They are too small to identify them as magnetite or wüstite morphologically. Metallic iron is present, but in smaller quantities than some other slags. Corroded metallic iron foils observed in one part of the sample. Very fine sulphide prills are present throughout the sample in the interstices between the fayalite laths.
8006	Classical/ Hellenistic	TS	None	X	XX	—	—	—	Slag dominated by iron silicate (likely fayalite) phases and hercynite. In places, the rims of the hercynite seem to be converting to another iron oxide. One tiny prill of metallic iron observed.
8007	Classical/ Hellenistic	TS	None	XX	XX	(see description)	—	—	Fayalite and iron metal dominated slag. Abundant foils of iron metal may replicate original ore morphologies.
8009	Classical/ Hellenistic	FS	None	XX	XX	XX	—	—	Significant metallic iron with a variety of morphologies, often corroded. Relict ore morphologies present in iron oxides

									(corroded metallic iron?) intergrown with silicates. Fayalite and hercynite present as freshly formed phases, but most iron oxides appear to be corroded metallic iron aggregates.
8010	Classical/ Hellenistic	FS	—	XX	—	X	—	—	Slag with thin iron silicate laths, virtually no free iron oxides, and many small, rounded prills of metallic iron. At least one large partially reacted ore-gangue fragment is present, identified by silica rich matrix and clusters of metallic iron particles.
8302	Classical/ Hellenistic	FS	—	—	—	—	—	—	Thin iron silicate laths in non-crystalline or microcrystalline groundmass.
8303	Classical/ Hellenistic	TS	—	XX	—	—	—	—	Glassy slag with numerous small, frequently rounded particles of metallic iron. Virtually no crystalline silicate phases. Very similar to 8305.
8304	Classical/ Hellenistic	I	—	XX	—	XX			Glassy slag with prills of metallic iron. Iron prills are dispersed within a more silica-enriched matrix in a texture suggesting it is a relict ore-gangue fragment where the iron has been reduced and liquified, and the silica has been partially melted. Iron oxides virtually absent.
8305	Classical/ Hellenistic	I	—	XX	—	—	—	—	Glassy slag with numerous small, frequently rounded particles of metallic iron. Virtually no crystalline silicate phases. Very similar to 8303.
8306	Classical/ Hellenistic	FS	Wüstite	XX	XX	—	XX	—	Wüstite and fayalite present in significant quantities. Numerous small particles of metallic iron. Iron sulphides and leucite were also observed. Iron sulphide phases are definitely present.
8307	Classical/ Hellenistic	FS	—	X	—	—	—	—	Thin iron silicate laths in non-crystalline or microcrystalline groundmass. A few small particles/prills of metallic iron.
8308	Classical/ Hellenistic	I	—	—	XX	—	—	—	Fayalite-dominated slag with piece of minimally-reacted technical ceramic. Al-rich spinels visible near technical ceramic.
8401	Medieval	FS/SHB	Wüstite	XX	XX	—	—	—	Wüstite- and fayalite-dominated slag containing small particles of metallic iron throughout. Somewhat corroded. Abundant Al-rich spinels.

8402	Medieval	FS/SHB	Wüstite	XX	XX	—	—	—	Wüstite-dominated slag with fayalite, also containing small particles of metallic iron throughout. Somewhat corroded.
8403	Medieval	TS	—	X	X	—	—	—	Fayalite-dominated slag with a few small prills of iron. Tapping band.

SEM-EDS chemical analysis of slags complements microscopic and mineralogical analysis, providing further details about the technological process (**table S4**). Areas analyses were conducted on at least four areas and averaged together. Corroded areas, unmelted inclusions, and gas bubbles were avoided wherever possible. For slags containing very large aggregates of metallic iron, two different sets of analyses were taken. One, avoiding the metallic iron aggregates, was intended to characterize the composition of the molten portion of the slag. The other, which included areas with metallic iron aggregates, was intended to approximate the overall composition of both the slag and metal.

Instead of binary plots, it is often useful to plot slag chemistry on a ternary phase diagram to understand the behaviour of the melt (**figure S7**). Such plots are very much approximations, as they ignore other elements that are present in the slags, and most phase diagrams are based on equilibrium conditions, which do not occur in ancient smelting furnaces. Nonetheless, because slag chemistry, especially the relative proportions of iron and silicon, is correlated with the redox conditions in the furnace and the carbon content of the metallic product (Tylecote *et al.* 1971, Rehder 2000:125-126, Rehren *et al.* 2007), such plots can be useful. Two phase diagrams commonly used to plot iron slag data were used, the SiO_2-FeO-Al_2O_3 diagram for low-calcium slags and the SiO_2-FeO-Anorthite ($CaAl_2Si_2O_8$) diagram for higher calcium slags (Morton & Wingrove 1972, 1969, Rehren *et al.* 2007, Charlton *et al.* 2010). MnO content was added to FeO content for the purposes of the phase diagram, given their similar behaviour in slag melts. Compositions were converted to anorthite from the oxide wt.% values by calculating the maximum wt.% of anorthite that could form given the existing calcium, aluminium, and silicon content of the slag. For each sample, the preferred ternary phase diagram for display was chosen based on which ternary sum account for a greater proportion of the actual composition (in most cases 85-95% of the total EDS normalized composition). For each sample, in order to plot them on a ternary diagram, values for the chosen three components were normalized to that they added to 100%.

Ternary plots of slag chemistries reveal that a substantial number cluster around the low-iron eutectic in the SiO_2-FeO-Al_2O_3 phase diagram, a slag composition that is typically correlated with higher reducing conditions in the furnace, higher carbon content in the resulting iron, and higher fuel to ore ratios in the furnace charge (Charlton *et al.* 2010:356-357). These results are consistent with the identification of mostly or completely vitreous slags, the

prevalence of metallic iron over iron oxides, and metallographic evidence suggesting the production of some liquid iron in these furnaces.

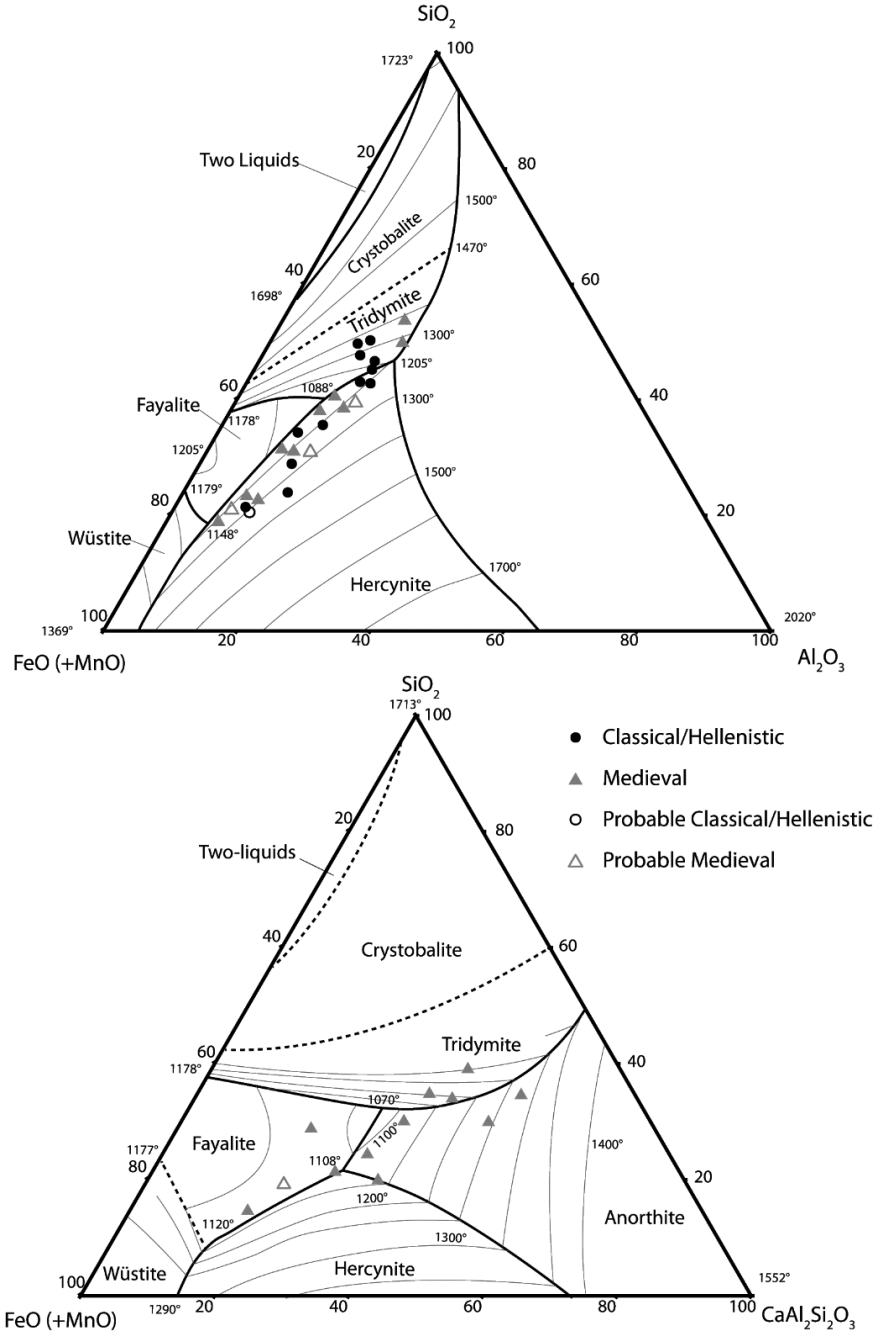

Figure S7. Plots of slag chemistries as measured by SEM-EDS on ternary phase diagrams. For samples with large aggregates of solid metallic iron, only analyses avoiding these aggregates are plotted. Note that melting temperatures and the phases indicated on the diagram represent an idealized ternary system at equilibrium. Since slags are not formed in equilibrium conditions and contain other elements, slag melting temperatures would have differed from those indicated on the diagram, and some of the phases indicated on the diagrams do not typically form in slags.

The composition of the ore fragments was also measured by SEM-EDS area analyses (**table S5**), but one should keep in mind that this does not include the weight of any lighter elements (e.g. hydrogen) bound up in iron hydroxides. Moreover, some of the ore samples (e.g. 6611) were extremely heterogeneous, with some areas higher in quartz, and others higher in iron oxides. As a result, these values should be interpreted more qualitatively than quantitatively.

The compositions of five glassy slags (5910, 5911, 6606, 8303, 8304, 8305) were also measured by wavelength-dispersive electron microprobe at the Research Lab for Archaeology and the History of Art at Oxford (**table S6**). Several spots on each sample were measured, avoiding any non-molten inclusions. Agreement with EDS area analyses was good.

Table S4. Normalized SEM-EDS area analyses of slag. The abbreviation "bdl" indicated "below detection limit" which was conservatively estimated through empirical observation of spectra at 0.2 or 0.3 wt.%.

Sample #	Site #	Na_2O	MgO	Al_2O_3	SiO_2	P_2O_5	SO_2	K_2O	CaO	TiO_2	MnO	FeO	CuO	ZnO	BaO
5701	57	0.8	1.8	14.2	28.2	1.6	0.3	1.4	2.3	0.6	bdl	48.8	bdl	bdl	bdl
5702	57	0.8	1.6	16.1	35.3	1.3	bdl	1.9	4.4	0.7	bdl	37.9	bdl	bdl	bdl
5801	58	0.5	1.1	8.1	19.4	1.6	0.4	1.6	2.3	bdl	bdl	65.0	bdl	bdl	bdl
5802	58	0.8	1.1	9.5	25.8	1.1	0.5	1.6	3.8	0.5	bdl	55.2	bdl	bdl	bdl
5901	59	0.4	0.6	7.4	17.9	0.4	0.7	1.1	2.1	bdl	bdl	69.5	bdl	bdl	bdl
5902	59	0.5	1.0	10.8	30.3	1.1	0.5	3.1	5.0	0.6	bdl	47.1	bdl	bdl	bdl
5903	59	1.9	1.4	17.2	43.0	1.3	0.7	2.3	5.3	0.9	bdl	26.1	bdl	bdl	bdl
5904 (no metal)	59	1.1	3.4	13.9	41.0	1.9	0.7	5.7	11.6	0.7	0.3	19.6	bdl	bdl	bdl
5904 (incl. metal)	59	0.9	4.3	11.1	31.2	2.0	0.5	3.6	11.0	0.5	0.3	34.5	bdl	bdl	bdl
5906	59	1.7	3.0	17.9	48.7	0.8	bdl	3.4	8.6	1.0	0.3	14.6	bdl	bdl	bdl
5907	59	0.9	1.1	14.8	34.1	1.0	0.5	2.7	5.0	0.5	bdl	39.6	bdl	bdl	bdl
5910	59	1.0	1.5	13.3	39.9	1.2	0.4	2.9	6.0	0.8	bdl	33.0	bdl	bdl	bdl
5911	59	0.5	1.1	13.1	36.9	0.6	0.3	2.8	3.2	0.7	bdl	40.9	bdl	bdl	bdl
5912 (no metal)	59	1.6	1.7	15.8	44.4	1.1	0.6	2.6	6.8	0.9	bdl	24.3	bdl	bdl	bdl
5912 (incl. metal)	59	1.3	1.5	13.5	37.0	0.8	0.4	2.4	4.6	0.7	bdl	37.7	bdl	bdl	bdl
5913	59	0.7	0.9	10.2	34.0	0.8	0.3	2.3	3.7	0.6	bdl	46.6	bdl	bdl	bdl
5914	59	0.7	1.1	10.6	35.4	0.7	0.4	2.1	5.9	0.7	bdl	42.5	bdl	bdl	bdl
6603 (no metal)	66	1.2	1.7	15.6	41.5	2.3	1.1	4.6	5.8	0.7	0.2	25.3	bdl	bdl	bdl
6603 (incl. metal)	66	1.0	1.3	13.6	33.8	1.6	0.9	4.0	4.3	0.6	bdl	38.9	bdl	bdl	bdl
6604 (no metal)	66	0.7	1.1	11.3	31.1	1.9	1.3	4.5	6.8	0.5	bdl	40.8	bdl	bdl	bdl
6604 (incl. metal)	66	0.6	1.0	9.3	23.1	1.8	1.1	2.7	5.6	0.5	bdl	54.3	bdl	bdl	bdl
6605 (no metal)	66	1.2	1.7	16.7	48.4	1.2	0.8	2.6	6.7	0.9	bdl	19.8	bdl	bdl	bdl
6605 (incl. metal)	66	1.0	1.2	13.3	34.7	1.0	1.4	1.7	4.7	0.7	bdl	40.5	bdl	bdl	bdl
6606 (no metal)	66	0.7	1.9	16.2	47.6	1.0	0.2	3.4	3.2	0.9	bdl	24.8	bdl	bdl	bdl
6606 (incl. metal)	66	0.5	1.3	10.7	28.7	1.6	0.2	1.8	1.8	0.4	bdl	52.9	bdl	bdl	bdl
6607	66	0.7	0.7	9.1	21.6	1.9	0.3	1.3	2.2	0.3	bdl	61.9	bdl	bdl	bdl
6608	66	0.8	0.7	10.1	28.8	0.9	0.6	2.4	2.5	0.5	bdl	52.7	bdl	bdl	bdl
6609	66	1.1	1.3	12.1	34.2	0.7	1.7	1.9	2.8	0.6	0.2	43.5	bdl	bdl	bdl
7901	79	0.2	0.4	11.4	20.1	bdl	bdl	0.4	1.0	0.5	bdl	66.2	bdl	bdl	bdl
8004	80	bdl	0.5	15.4	23.6	bdl	bdl	0.4	0.2	0.5	0.3	59.1	bdl	bdl	bdl
8005	80	0.3	0.4	11.6	33.3	0.2	0.2	0.8	0.3	0.8	0.2	51.9	bdl	bdl	bdl
8006	80	0.2	0.4	13.5	28.3	0.2	bdl	0.6	0.2	0.7	0.8	55.2	bdl	bdl	bdl
8007	80	0.2	0.4	14.6	34.7	0.2	0.2	0.8	0.3	0.8	1.3	46.6	bdl	bdl	bdl
8009	80	0.2	0.5	17.1	43.9	bdl	0.2	0.9	0.3	0.9	2.8	33.2	bdl	bdl	bdl

8302	83	1.1	1.4	13.3	43.5	0.8	0.3	1.8	2.8	0.6	1.7	32.6	bdl	bdl	bdl
8303	83	0.9	2.6	11.9	44.6	0.7	0.4	1.6	3.5	0.6	1.3	31.8	bdl	bdl	bdl
8304	83	bdl	0.8	17.8	41.0	0.7	bdl	0.8	0.7	1.0	1.8	35.1	bdl	bdl	0.3
8305	83	1.0	1.5	14.0	47.3	0.5	bdl	1.6	0.8	0.7	0.8	31.9	bdl	bdl	bdl
8306	83	0.2	0.9	10.3	20.8	0.2	0.6	0.4	0.5	0.3	0.4	65.4	bdl	bdl	bdl
8307	83	0.6	0.8	16.1	41.0	0.6	bdl	1.5	0.5	0.8	0.7	37.4	bdl	bdl	bdl
8308	83	0.8	1.1	16.3	44.0	0.6	bdl	1.4	1.2	0.7	0.7	33.2	bdl	bdl	bdl
8401	84	0.2	0.7	11.5	21.9	0.2	0.2	1.0	0.8	0.4	0.3	62.9	bdl	bdl	bdl
8402	84	0.4	0.6	7.0	21.4	0.4	bdl	1.2	3.4	0.3	bdl	65.4	bdl	bdl	bdl
8403	84	0.3	0.6	12.5	29.9	bdl	bdl	1.1	1.1	0.5	0.7	53.2	bdl	bdl	bdl

Table S5. Normalized SEM-EDS area analyses of ores. Note that iron ores may contain significant hydroxides and other light elements which are not detected by SEM-EDS. The abbreviation "bdl" indicated "below detection limit" which was conservatively estimated through empirical observation of spectra at 0.2 or 0.3 wt.%.

Sample #	**Site #**	**Na_2O**	**MgO**	**Al_2O_3**	**SiO_2**	**P_2O_5**	**SO_2**	**K_2O**	**CaO**	**TiO_2**	**MnO**	**FeO**	**CuO**	**ZnO**	**BaO**
5905	59	bdl	bdl	2.4	20.1	bdl	0.3	bdl	bdl	0.4	bdl	76.9	bdl	bdl	bdl
5908	59	bdl	0.3	2.6	6.0	bdl	0.6	bdl	bdl	bdl	bdl	90.5	bdl	bdl	bdl
5909	59	bdl	bdl	4.9	31.2	0.3	0.3	0.3	bdl	0.6	bdl	62.4	bdl	bdl	bdl
6601	66	bdl	bdl	0.6	23.5	0.3	0.3	bdl	0.2	1.1	bdl	74.0	bdl	bdl	bdl
6610	66	0.4	0.2	7.7	43.7	0.5	2.7	0.9	0.3	0.8	bdl	42.9	bdl	bdl	bdl
6611	66	0.7	0.6	13.5	41.1	0.5	0.6	1.8	0.3	0.9	bdl	40.0	bdl	bdl	bdl
6612	66	0.3	0.4	11.9	41.7	0.7	0.2	1.9	0.3	0.7	bdl	42.0	bdl	bdl	bdl
8301	83	bdl	bdl	5.9	25.6	bdl	bdl	0.2	bdl	0.4	0.3	67.6	bdl	bdl	bdl

Table S6. WDS microprobe spot analyses of vitreous slags (wt.%). Data were normalized, but the non-normalized analytical totals are reported as well. Multiple spots were analysed on each sample. Detection limit for SO_2 is 0.06, while CuO is 0.1.

Sample #	**Spot #**	**Na_2O**	**MgO**	**Al_2O_3**	**SiO_2**	**P_2O_5**	**SO_2**	**K_2O**	**CaO**	**TiO_2**	**MnO**	**FeO**	**CuO**	**Total (non-normalized)**
5910	1	1.05	1.60	12.83	40.81	1.18	0.14	2.93	6.70	0.84	0.16	31.75	bdl	93.29
5910	2	1.16	1.76	14.03	42.30	1.24	0.15	3.03	6.49	0.75	0.13	28.95	bdl	95.95
5910	3	1.13	1.92	13.38	41.50	1.28	0.10	3.03	5.62	0.84	0.10	31.11	bdl	95.23
5910	4	1.09	1.74	13.28	41.84	1.24	0.13	3.06	6.71	0.75	0.11	29.91	0.15	95.64
5910	5	1.09	1.61	13.20	42.15	1.22	0.13	2.75	6.90	0.90	0.19	29.84	bdl	93.59
5910	6	1.17	1.85	13.14	42.24	1.18	0.13	2.85	6.75	0.80	0.15	29.73	bdl	95.45

5911	1	0.48	1.05	13.30	39.27	0.64	0.10	2.86	3.44	0.81	0.04	38.02	bdl	96.72
5911	2	0.40	1.01	13.19	39.04	0.68	0.10	2.94	3.34	0.80	0.04	38.46	bdl	96.09
5911	3	0.50	1.03	13.36	39.83	0.72	0.11	3.02	3.53	0.84	0.13	36.93	bdl	96.04
5911	4	0.55	1.00	13.28	39.57	0.66	0.09	2.95	3.48	0.81	0.07	37.55	bdl	95.32
5911	5	0.43	0.94	13.03	39.30	0.64	0.11	2.90	3.20	0.82	0.13	38.50	bdl	96.26
5911	6	0.39	0.99	13.04	38.77	0.70	0.10	2.79	3.35	0.73	0.05	39.09	bdl	96.48
6606	1	0.82	1.81	17.52	52.23	0.71	bdl	4.18	3.33	0.94	0.08	18.37	bdl	97.18
6606	2	0.76	1.94	17.58	51.07	0.74	bdl	3.71	3.40	0.98	0.07	19.75	bdl	96.59
6606	3	0.92	1.88	17.84	51.52	0.84	0.07	4.00	3.34	0.95	0.14	18.49	bdl	97.15
6606	4	0.64	1.96	18.16	50.82	0.86	bdl	3.90	4.01	0.95	0.15	18.56	bdl	96.71
6606	5	0.85	1.97	18.46	52.68	0.83	bdl	4.01	3.45	1.02	0.07	16.66	bdl	97.10
8303	1	0.69	2.44	12.22	46.56	0.66	0.15	1.72	3.55	0.68	1.42	29.90	bdl	95.99
8303	2	0.85	2.48	11.92	47.10	0.64	0.13	1.77	3.53	0.68	1.46	29.45	bdl	95.33
8303	3	0.55	2.62	11.33	43.82	0.74	0.15	1.30	3.60	0.71	1.47	33.72	bdl	96.01
8303	4	0.76	2.47	11.89	46.18	0.68	0.14	1.69	3.60	0.69	1.52	30.37	bdl	95.91
8303	5	0.73	2.49	12.34	48.41	0.60	0.14	1.87	3.62	0.64	1.37	27.79	bdl	96.40
8303	6	0.93	2.45	12.01	46.52	0.69	0.14	1.75	3.58	0.68	1.36	29.89	bdl	95.46
8304	1	0.11	0.73	17.86	42.32	0.63	bdl	0.96	0.76	1.05	1.97	33.62	bdl	95.67
8304	2	0.13	0.79	18.25	42.35	0.63	bdl	0.98	0.76	1.09	1.89	33.14	bdl	94.23
8304	3	0.04	0.74	17.75	41.96	0.71	bdl	0.92	0.62	1.05	1.79	34.42	bdl	94.79
8304	4	0.15	0.72	17.74	41.22	0.71	bdl	0.81	0.66	1.07	1.82	35.12	bdl	94.98
8304	5	0.10	0.80	18.11	42.56	0.68	bdl	1.00	0.75	1.07	1.80	33.14	bdl	95.28
8304	6	0.15	0.74	17.96	41.92	0.71	bdl	0.84	0.62	1.06	1.83	34.17	bdl	94.51
8305	1	1.02	1.26	14.50	49.60	0.47	bdl	1.64	0.80	0.82	0.90	28.98	bdl	96.18
8305	2	0.82	1.29	14.18	49.55	0.48	bdl	1.59	0.78	0.76	0.72	29.83	bdl	95.82
8305	3	0.80	1.34	14.17	49.53	0.49	bdl	1.60	0.79	0.78	0.88	29.61	bdl	96.81
8305	4	0.94	1.39	14.02	49.32	0.43	bdl	1.61	0.85	0.79	0.88	29.78	bdl	95.83
8305	5	0.78	1.35	14.01	49.10	0.53	bdl	1.62	0.80	0.73	0.87	30.21	bdl	95.91
8305	6	0.98	1.39	14.17	49.18	0.46	bdl	1.68	0.83	0.74	0.80	29.79	bdl	96.76

References

CHARLTON, M.F., CREW, P., REHREN, T. & SHENNAN, S.J. 2010. Explaining the evolution of ironmaking recipes – An example from northwest Wales. *Journal of Anthropological Archaeology* 29: 352-367.

ERB-SATULLO, N.L., GILMOUR, B.J.J. & KHAKHUTAISHVILI, N. 2015. Crucible technologies in the Late Bronze-Early Iron Age South Caucasus: Copper processing, tin bronze production, and the possibility of local tin ores. *Journal of Archaeological Science* 61: 260-276.

—. 2018. The ebb and flow of copper and iron smelting in the South Caucasus. *Radiocarbon* 60: 159-180.

KHAKHUTAISHVILI, D.A. 2009. *The Manufacture of Iron in Ancient Colchis*. (BAR International Series series 1905). Oxford: Archaeopress.

MORTON, G.R. & WINGROVE, J. 1969. Constitution of bloomery slags: Part I: Roman. *Journal of the Iron and Steel Institute* 207: 1556-1564.

—. 1972. Constitution of bloomery slags: Part II: Medieval. *Journal of the Iron and Steel Institute* 210: 478-488.

MURALHA, V.S.F., REHREN, T. & CLARK, R.J.H. 2011. Characterization of an iron smelting slag from Zimbabwe by Raman microscopy and electron beam analysis. *Journal of Raman Spectroscopy* 42: 2077-2084.

REHDER, J.E. 2000. *Mastery and Uses of Fire in Antiquity*. Montreal and Kingston: McGill-Queen's University Press.

REHREN, T., CHARLTON, M., CHIRIKURE, S., HUMPHRIS, J., IGE, A. & VELDHUIZJEN, H.A. 2007. Decisions set in slag--the human factor in African iron smelting, in S. LANIECE, D. HOOK & P. CRADDOCK (eds.) *Metals and Mines--Studies in Archaeometallurgy*: 211-218. London: Archetype.

TYLECOTE, R.F., AUSTIN, J.M. & WRAITH, A.E. 1971. The mechanism of the bloomery process in the shaft furnaces. *Journal of the Iron and Steel Institute* 209: 243-363.

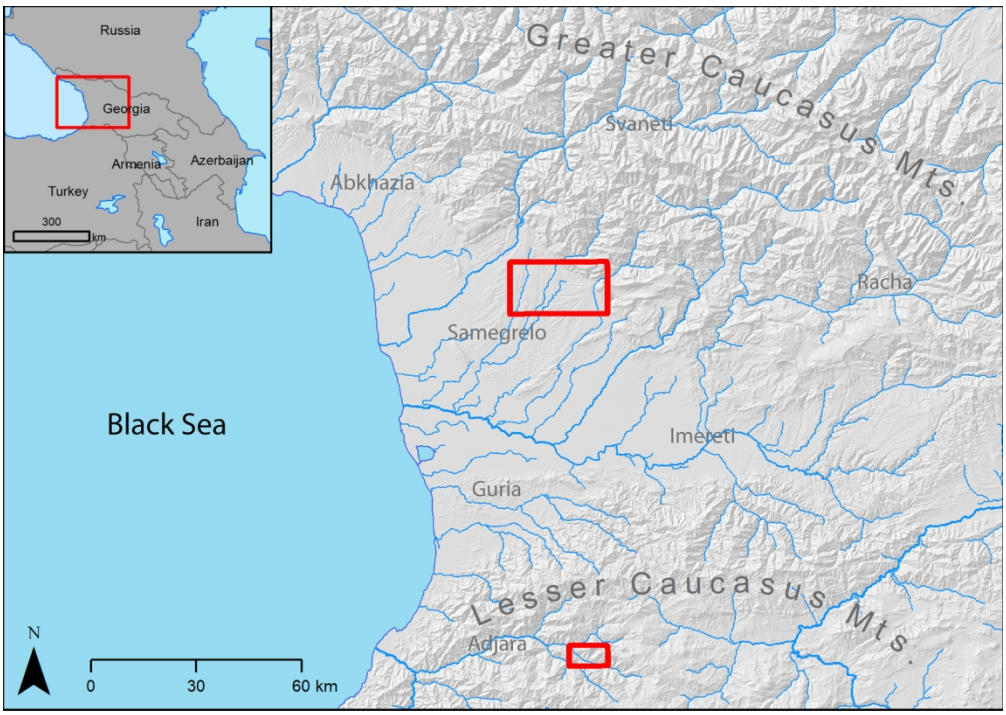

Figure 1. Map of the eastern Black Sea area showing survey areas (see figure 2) and modern region names.

134x95mm (300 x 300 DPI)

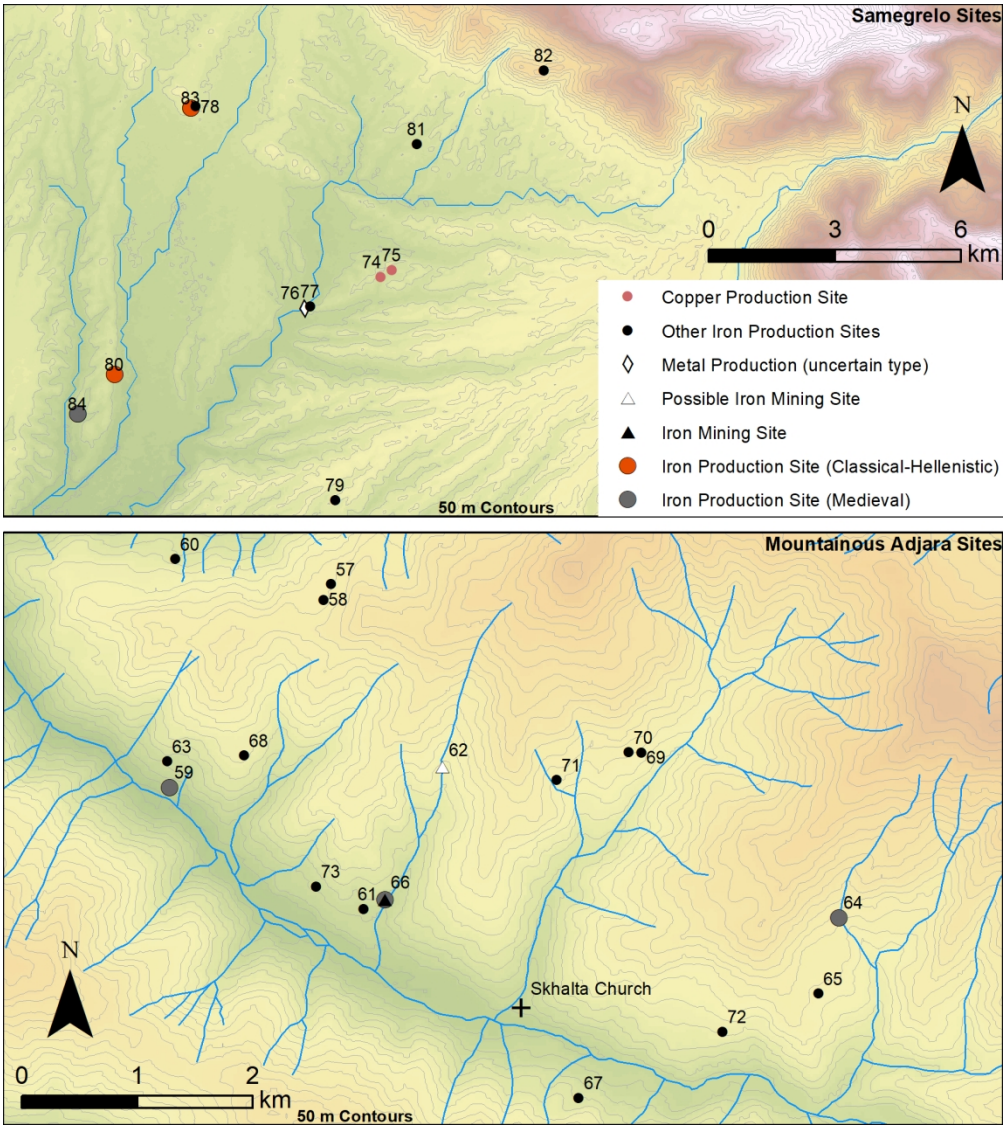

Figure 2. Maps of metal production sites in highland Adjara and Samegrelo.

158x177mm (300 x 300 DPI)

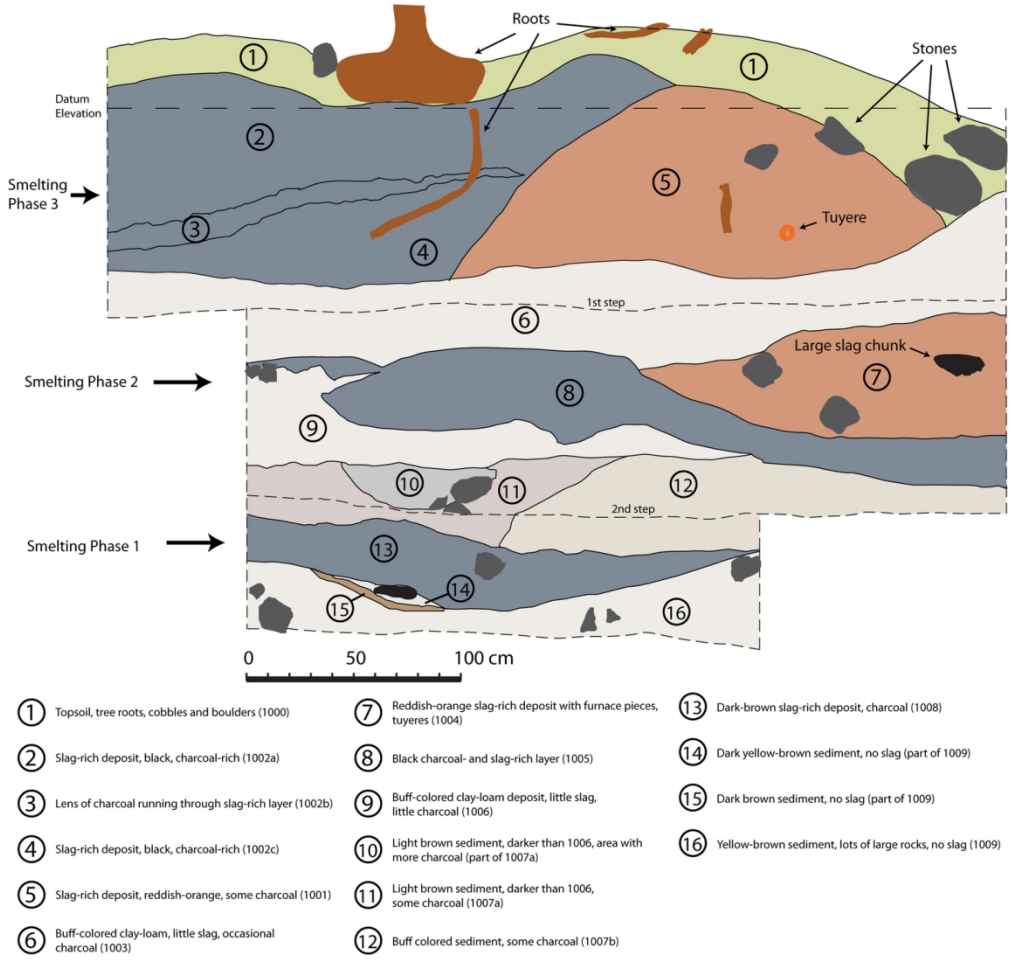

Figure 3. Drawing of section exposed by modern road cut at Site 59.

134x128mm (300 x 300 DPI)

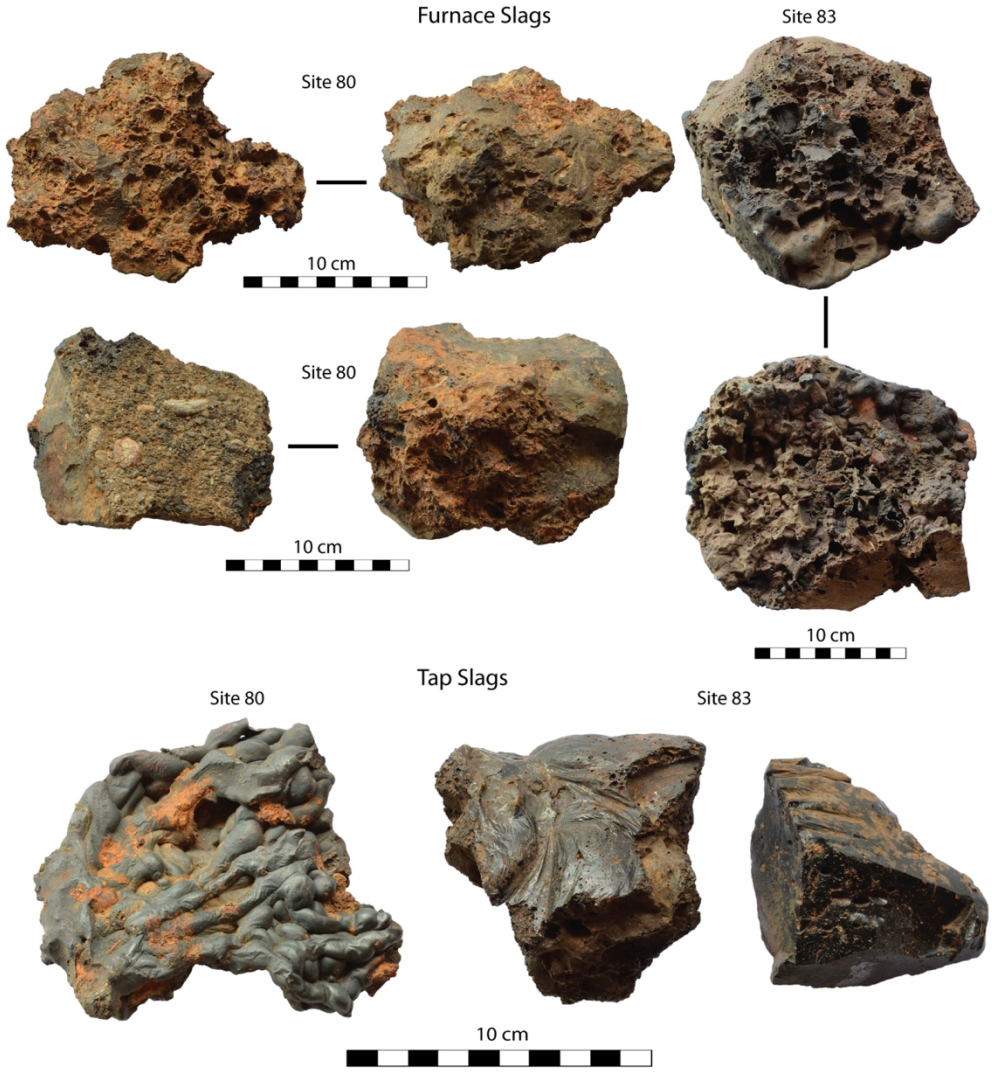

Figure 4. Slags from Classical/Hellenistic sites. Two examples of glassy slag are shown at the bottom right.

134x151mm (300 x 300 DPI)

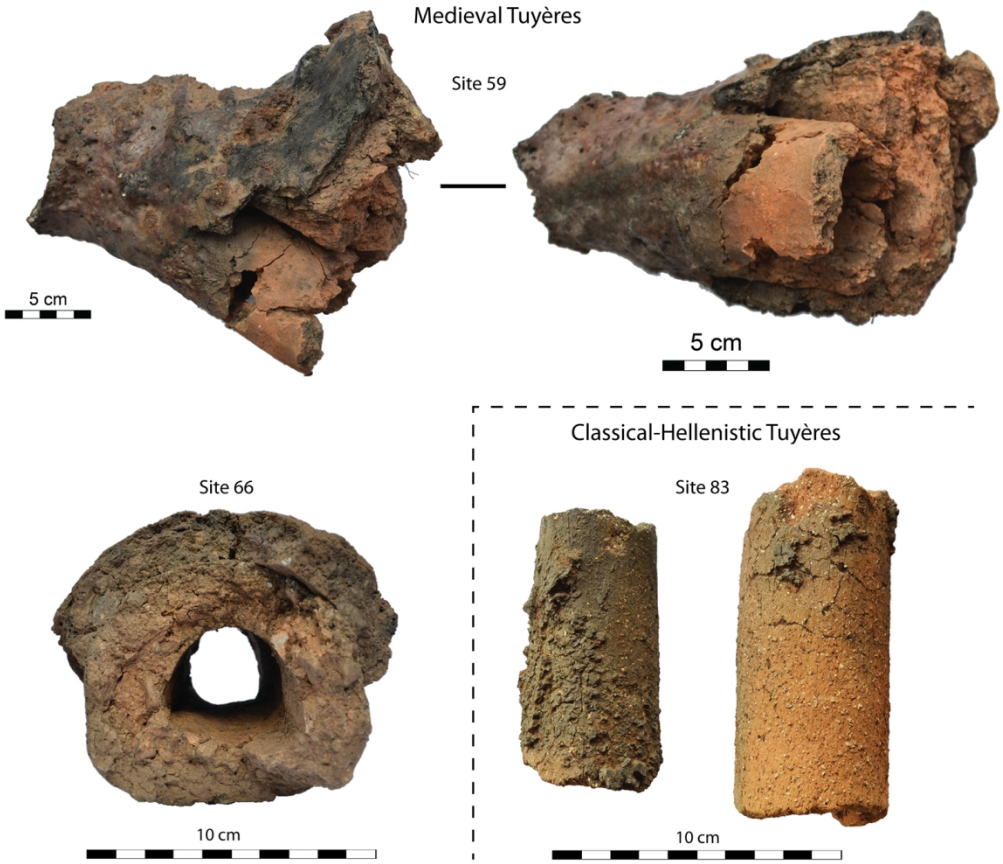

Figure 5. Examples of Medieval and Classical-Hellenistic tuyères with fused furnace material.

134x119mm (300 x 300 DPI)

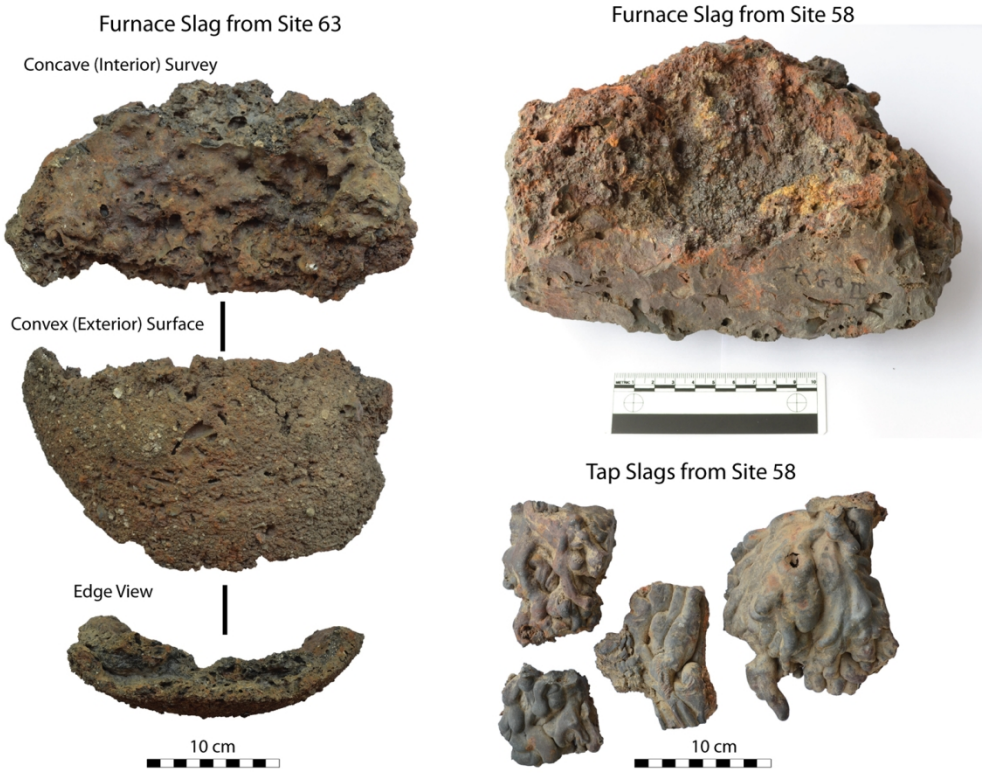

Figure 6. Furnace and tap slags from Medieval smelting sites.

134x107mm (300 x 300 DPI)

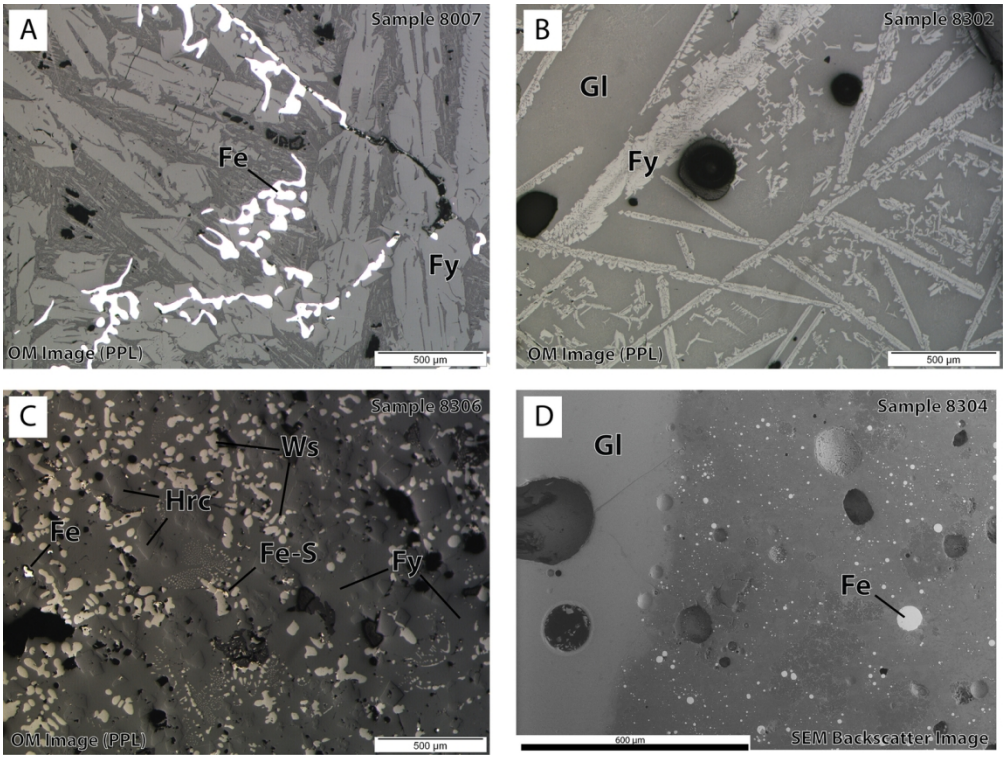

Figure 7. Microstructures of Classical-Hellenistic slags from Sites 80 (A) and 83 (B-D) in Samegrelo. Abbreviations: Fe – metallic iron, Fy – fayalite, Ws – wüstite, Fe-S – iron sulphide, Hrc – hercynite, Gl – glassy phase.

134x101mm (300 x 300 DPI)

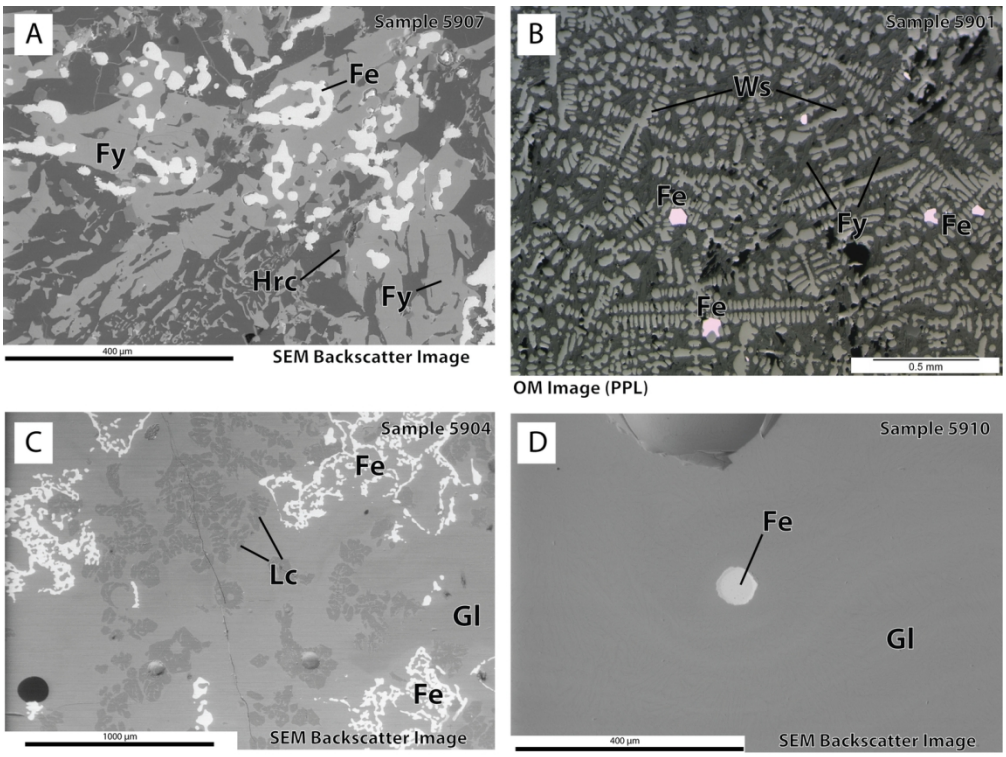

Figure 8. Microstructures of Medieval slags from Site 59 in Adjara. Abbreviations: Abbreviations: Fe – metallic iron, Fy – fayalite, Ws – wüstite, Fe-S – iron sulphide, Hrc – hercynite, Lc – leucite, Gl – glassy phase.

134x102mm (300 x 300 DPI)

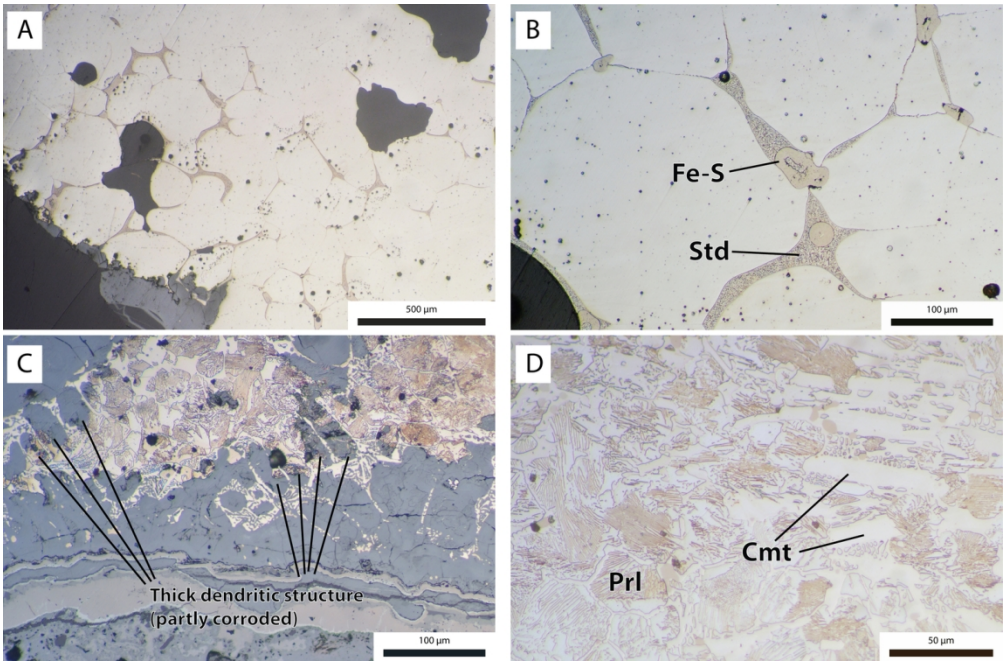

Figure 9. Optical photomicrograph of iron aggregates in samples 6606 (A and B) and 5904 (C and D) from highland Adjara. Etched with Nital. Abbreviations: Fe-S – iron sulphide, Std – steadite, Prl – pearlite, Cmt – cementite.

134x88mm (300 x 300 DPI)

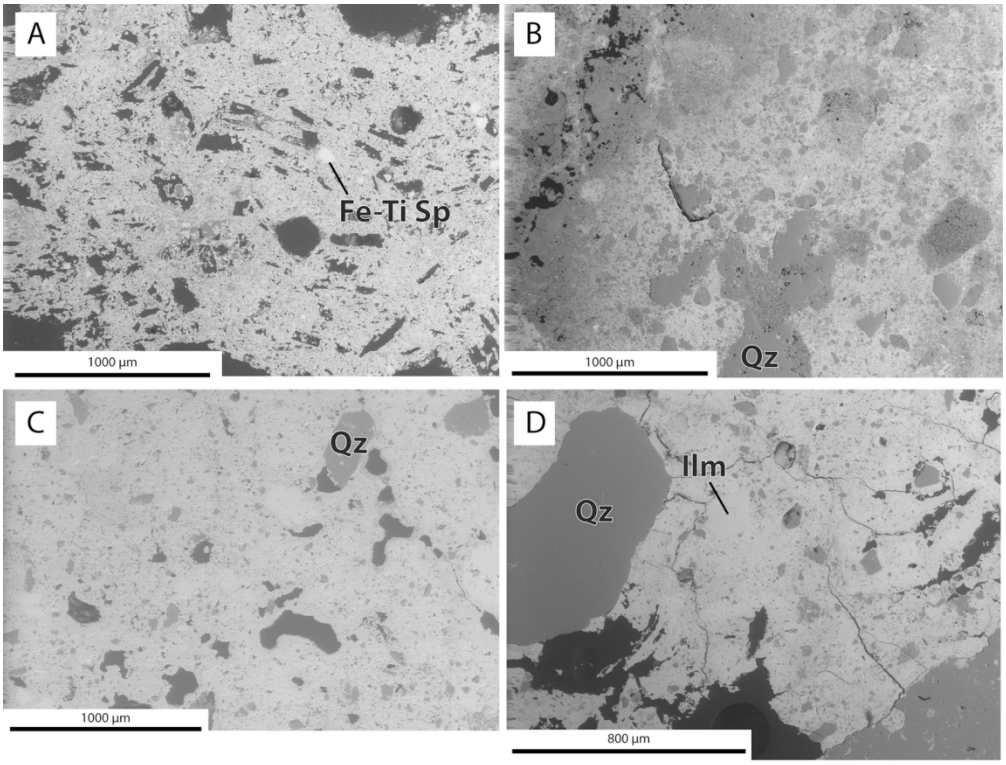

Figure 10. SEM images of ore samples from highland Adjara (A: Sample 6601, B: Sample 6610, C: Sample 5905) and Samegrelo (D: Sample 8301). Abbreviations: Qz – quartz, Ilm – ilmenite, Fe-Ti Sp – iron-titanium spinel.

134x103mm (300 x 300 DPI)